/ LEWIS / · / · / · /
/N - 33 -c R
7C 3425
P-86

Wisconsin Power Electronics Research Center

NASA Grant Report

HIGH POWER DENSITY DC/DC CONVERTER - COMPONENT SELECTION AND DESIGN

Grant No. NAG3-804
Interim Report

University of Wisconsin - Madison
Department of Electrical and Computer Engineering
1415 Johnson Drive
Madison, WI 53706

Deepakraj M. Divan
Principal Investigator

Mustansir H. Kheraluwala
Project Engineer

Prepared For

TABLE OF CONTENTS

CHAPTER 1

INTRODUCTION

1.1 Goal

This report, covering Phase 2 of this project, presents further work pertaining to design considerations for the new high power, high frequency dc/dc converters introduced in Phase 1. To reiterate, the goal of the project is the development of high power, high power density dc/dc converters at power levels in the multi-kilowatt to megawatt range for aerospace applications. The prototype converter is rated for 50 kW at a switching frequency of 50 kHz, with an input voltage of 200 Vdc and an output of 2000 Vdc. The overall power density must be in the vicinity of 0.2 - 0.3 kg/kW.

1.2 Review of Phase 1 of the Project

In Phase 1 of this project three new dc/dc converter topologies suitable for high power, high power density applications were proposed. The dual active bridge topology was seen to offer many desirable features including zero voltage switching on all semiconductor devices, bidirectional power flow, buck-boost operation, good range of control, effective use of system parasitics, and constant frequency operation. Based on an idealized model of the devices and the isolation transformer, the three topologies were analyzed to assess, in particular, their power flow versus control characteristics, transformer kVA versus power flow characteristics and to identify regions of operation, under soft switching, on the output voltage versus output current plane. Based on this analysis, a table of component stresses for the three topologies operating at the design point, was compiled. The single phase dual active bridge dc/dc converter (Topology B) was seen to offer minimal device stresses, and

simpler transformer with good utilization, and was, hence, justified as a viable option for the application.

1.3 Overview of Phase 2 of the Project

This report discusses design issues related to the choice of the switching device type, limitations/extensions on the soft switching region due to the transformer magnetizing inductance and device snubber capacitance, and finally design considerations for high power, high frequency transformers.

Much of the second chapter pertaining to the selection of the optimum converter topology, has been reported in Phase 1. Based on component stresses, the single phase dual active bridge dc/dc converter (Topology B) was seen to be an optimum choice. This choice is further supported from an analysis of converter losses, which includes device switching and conduction losses. The device types investigated are the state-of-the-art Insulated Gate Bipolar Transistor (IGBT) an the MOS Controlled Thyristor (MCT).

Chapter three deals with the influence of the transformer magnetizing inductance and the device snubber capacitance (required for zero voltage turn-off) on the soft switching regions on the output voltage versus output current plane. It is seen that the soft switching region expands with decreasing transformer magnetizing inductance. On the other hand, with increasing device snubber capacitance (necessary for reducing turn-off losses) this soft switching regions diminishes.

The transformer, required for galvanic isolation in high power converters, is seen to be a major component in the converter power density. Issues regarding selection of core material, influence of high frequency on copper losses and control of leakage inductance are investigated in chapter four. State-of-the-art high frequency core materials such as Ferrites, Permalloy 80 and Metglas have been

characterized for core losses at various operating frequencies and flux densities. Copper loss in three conventional winding arrangements have been evaluated, at the rated conditions. The requirement of a low and controllable leakage inductance, has led to the investigation of coaxially wound transformers, commonly used for radio frequency applications. Two such configurations, one with rectangular tube for the primary and the other with circular tube for the same, have been analyzed, fabricated and tested. The test results show that, indeed, very low leakage inductances in the order of a few nanohenries, can be realized.

In chapter five, experimental results obtained from a 1 kW proof-of-concept unit switching at 20 kHz (using Bipolar Junction Transistors) are presented. Conclusions and future work are also summarized here.

CHAPTER 2

SELECTION OF OPTIMUM CONVERTER TOPOLOGY

2.1   Introduction

With a knowledge of the performance characteristics of the various components in the three proposed topologies, presented in detail in the last chapter, we are now in a position to quantitatively assess the merits and demerits of these circuits. The final objective being to select one of these topologies which realizes the highest power density, for the given rated specifications, under minimal component stresses, device losses and control complexity. These issues are investigated based on the consideration that each topology operates at its optimum transformer utilization at rated conditions of 50 kW, input dc voltage of 200V, output dc voltage of 2000V and a minimum switching frequency of 50 kHz.

Much of the following section has already been reported in Report Number 1, for the period July 1987 to June 1988 [1]. However, the selection of the final converter topology, Topology B, as was discussed in the first report, was based on considerations of component stresses only. In this phase of the project further work concerning converter losses, including switching and conduction losses were evaluated, at the optimum operating point for each of the proposed topologies. Section 2.3 outlines this work. Much of Section 2.4 is also repeated to summarize the previous work and also to add continuity to this phase of the project.

2.2   Comparison of Proposed Topologies Based on Considerations of Component Stresses

Figures 2.2.1a, b, c show the three converter topologies which were considered in the previous report [1]. Table 2.2.1 summarizes the results of the idealized component stress analyses carried out in
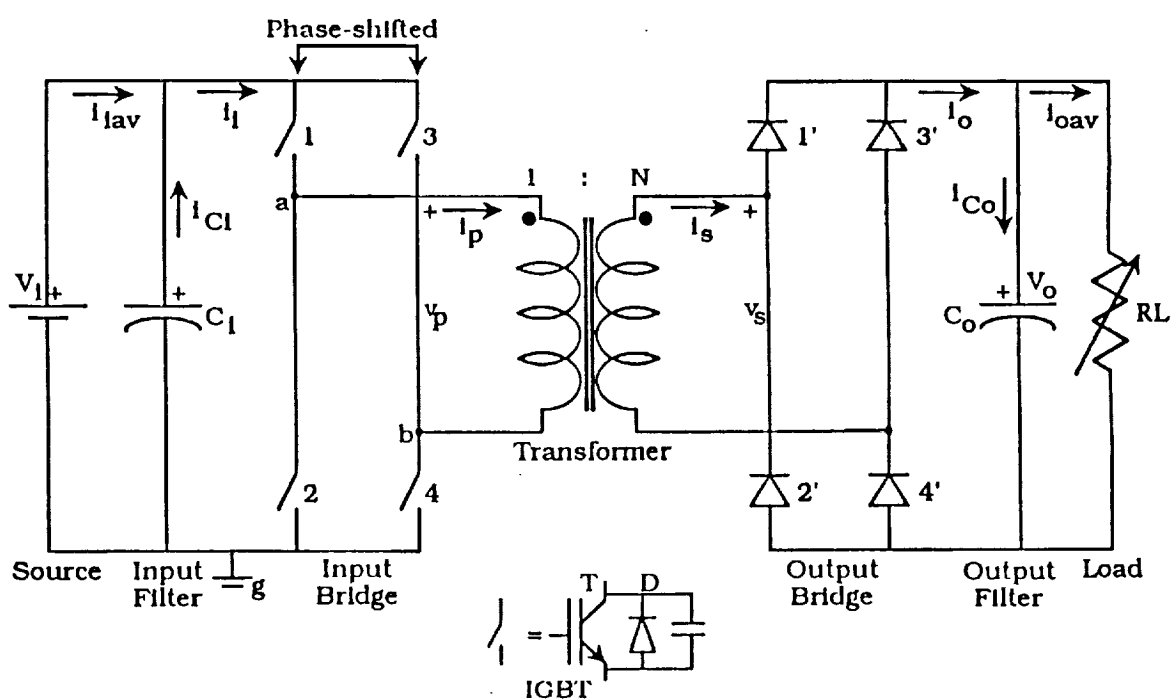
4

Figure 2.2.1a Schematic of Single Phase Single Active Bridge DC/DC Converter (Topology A)
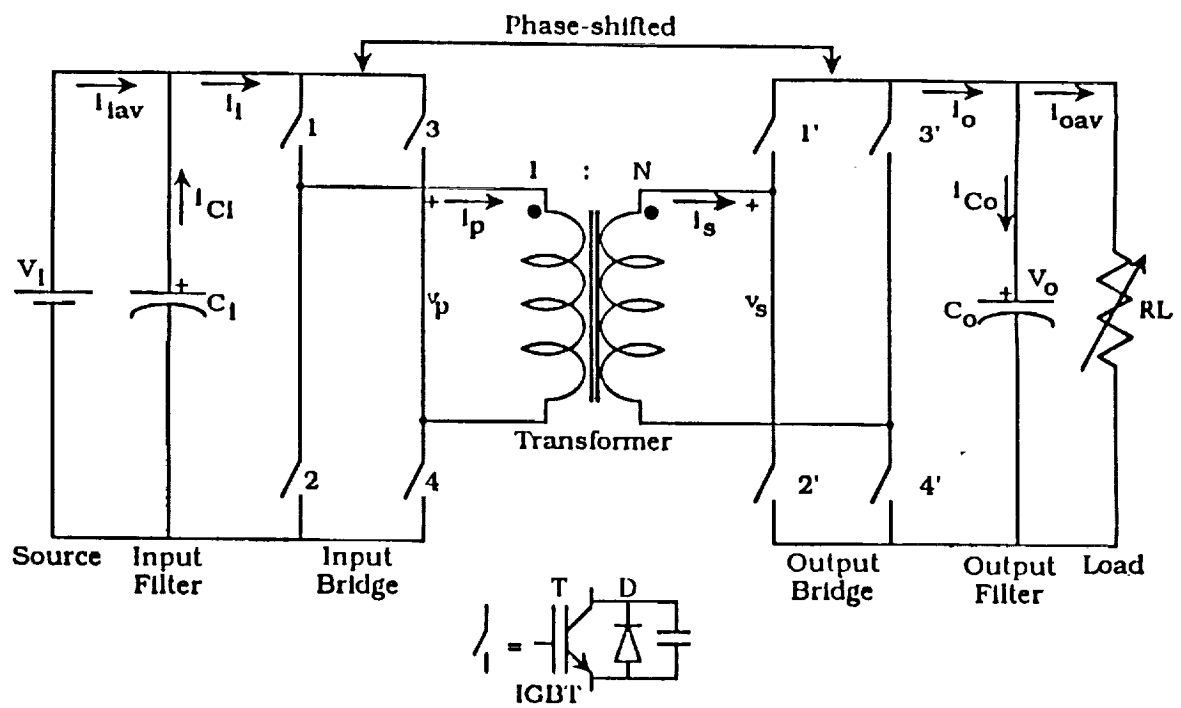
Figure 2.2.1b   Schematic of Single Phase Dual Active Bridge DC/DC Converter (Topology B)
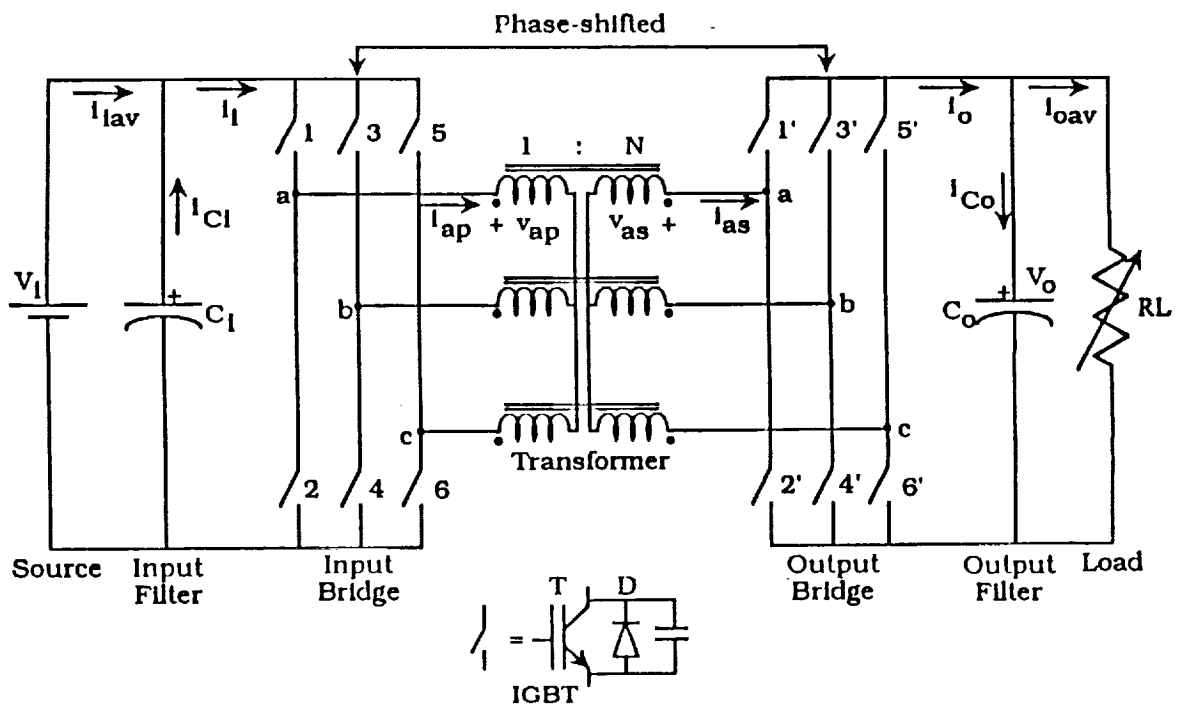
Figure 2.2.1c Schematic of Three Phase Dual Active Bridge DC/DC Converter (Topology C)

[1]. Converter design points have been chosen as per considerations in [1]. All converters are rated for 50 kW, switching at 50 kHz, with 200 Vdc input and 2000 Vdc output.

Examining the peak device stresses for each bridge, Topology C offers the lowest (V_{pk} * I_{pk} / P_o) stress at 1.17pu. However, Topology B shows a slightly higher stress of 1.19pu, with a saving of two devices on each bridge. Topology A exhibits very high device stresses on both the bridges. Infact, the 1.19pu device stress for Topology B compares favourably with the desired stress of 1pu, theoretically achievable with hard-switched pwm converters.

Comparing the transformer specifications, again Topology A seems to be poorest in regard to peak current stresses and transformer utilization. Both Topologies B and C offer almost identical performances. However, it must be emphasized that Topology C requires a three-phase transformer with identical equivalent leakage inductances in each phase. This is necessary for two reasons :

(i)   Balanced three-phase currents, resulting in current components at multiples of six times the switching frequency only, at the dc sides of the bridges. Hence, reduction in the RMS-current ratings of the filter capacitors, and

(ii)   The minimum current constraint for zero-voltage switching of the active devices at turn-off, is dictated by the value of

the leakage inductance and snubber capacitance. Hence, for this minimum current to be identical for each device, it is necessary that the leakage inductance be identical in each phase.

TABLE 2.2.1

(Summary of Component Stresses)

$(P_O = 50 \text{ kW} ; V_I = 200 \text{ Vdc} ; V_O = 2000 \text{ Vdc} ; f = 50 \text{ kHz})$

	Topology A	Topology B	Topology C
d	0.58	1	1
$\beta(°)$	180	-	-
$\phi(°)$	-	28.78	35.41
Device Specs.			
Input Bridge			
No. of Active Devices	4	4	6
Peak voltage(V)	200	200	200
Peak current(A)	861.48	297.57	293.46
$V_{pk}{}^*I_{pk} / P_O$	3.45	1.19	1.17
Output Bridge			
No. of Active Devices	4(diodes)	4	6
Peak voltage(V)	2000	2000	2000
Peak current(A)	50.68	29.76	29.35
$V_{pk}{}^*I_{pk} / P_O$	2.03	1.19	1.17
Transformer Specs.			
1 : N	1 : 17	1 : 10	1 : 10(Y-Y)
Peak pri. volts(V)	200	200	133/ph
Peak pri. amps(A)	861.48	297.57	293.46
RMS pri. amps(A)	497.52	281.4	197.29/ph
Peak sec. volts(V)	2000	2000	1333/ph
Peak sec. amps(A)	50.68	29.76	29.35
RMS sec. amps(A)	29.27	28.14	19.73/ph
kVA	78.64	56.28	55.7
P_O / kVA	0.64	0.89	0.89
$L(\mu H)$	0.77	1.1	0.89/ph
Filter Specs.			
Input			
Cap. volts(Vdc)	200	200	200
Cap. RMS amps(A)	429.75	129.15	48.43
kVA	85.95	25.83	9.69
Output			
Cap. volts(Vdc)	2000	2000	2000
Cap. RMS amps(A)	14.63	12.92	4.84
kVA	29.26	25.83	9.69
Operation	1-Quadrant	2-Quadrant	2-Quadrant
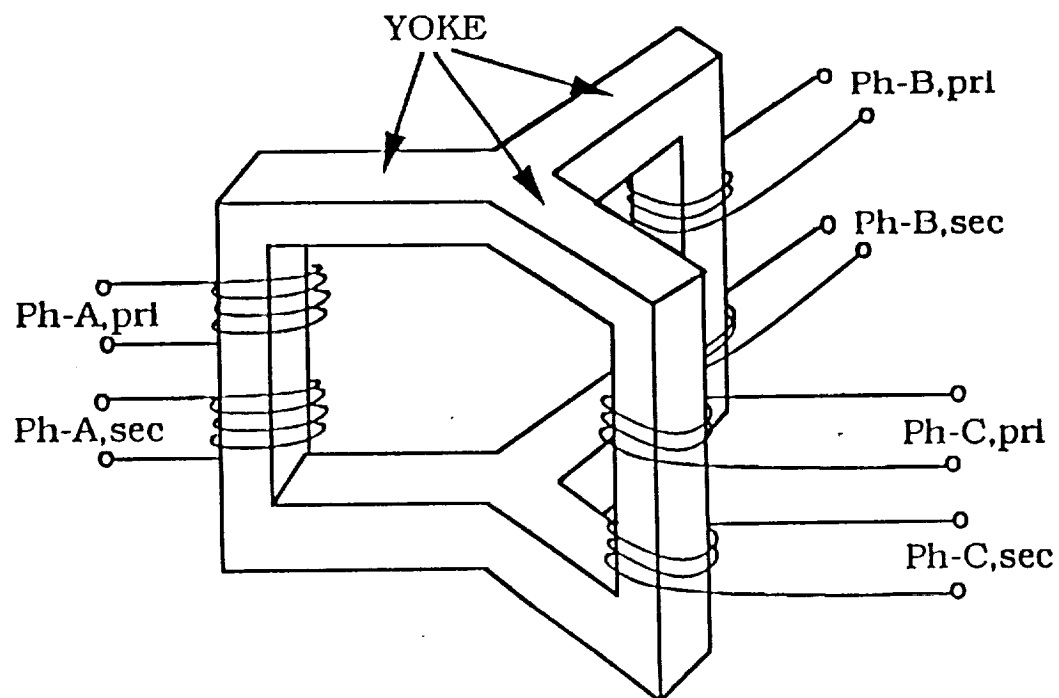
Figure 2.2.1   Schematic of a possible geometry of a Symmetrical 3-phase Transformer

Figure 2.2.2 shows a possible construction of such a symmetrical three-phase transformer. In view of the constraint of high power density, the non-conventional core geometry requiring additional yokes could be a difficult problem to resolve.

Finally, examining the input and output filter capacitor ratings, Topology C exhibits the lowest RMS-current stresses and hence, lowest kVA, for reasons mentioned above. Topology A is the worst with 9 times the kVA rating for that of the input capacitor for Topology C. However, the output filter stresses for Topology A are much lower than that of its input filter. This is because, the output bridge being a diode bridge allows the current on its dc side to be unidirectional only, resulting in lower ripple currents.

2.3   Comparison of Proposed Topologies Based on Considerations of Converter Losses

This section analyzes the device switching and conduction losses incurred in each of the proposed topologies [2]. A preliminary assessment of the three topologies indicates that, such an analysis for Topology C may not be worthwhile, since it has more devices (6 on each bridge as opposed to 4 for Topology B), it is more complex to control and may have lower overall efficiency. Hence, the analysis will only be carried Topologies A and B.

Converter losses are a strong function of switching frequency and switching methodology. As stated earlier, for high power density converters, operating at high frequencies, the use of zero-voltage/zero-current switching techniques so as to minimize the switching losses, is an attractive alternative. In the proposed topologies, all devices operate under conditions of zero-voltage switching. The turn-on of any device is initiated while its anti-parallel diode is conducting. This ensures that the device naturally takes over as the diode current reverses, and more importantly, does so under

almost zero-voltage conditions. The turn-off process must always be initiated when the device is carrying a certain minimum current. The rate of rise of voltage across the device during its turn-off is governed by the snubber capacitor. Typically, such circuits are oversnubbed to ensure near zero-voltage turn-off.

An extensive analysis was carried out to ascertain the switching and conduction losses. The device of choice at this time, is the Insulated Gate Bipolar Transistor(IGBT). Although the MOS Controlled Thyristor(MCT) seems to be a better alternative from a standpoint of speed and forward drop, availability of adequately rated devices is not anticipated in the near future. A typical model for the turn-off switching waveform is shown in Figure 2.3.1 [3]. I_m is the current at the instant of turn-off. The model shows that the current through the device comes down almost instantaneously to a value $K*I_m$, and then decays to zero over a time, tf, sometimes referred to as the tail time. The parameter, K is usually specified by the manufacturer as 0.25. With a knowledge of the turn-off behaviour, an expression for the turn-off losses is derived and is shown in Equation (2.3.1). The current through the leakage inductance is assumed to be constant over the small switching transition.

$$P_{sw} \text{ / device} = \frac{f \, I_m^2 \, t_f^2 \, (4 - 3K) \, K}{48 \, C} \qquad \text{...(2.3.1)}$$

where, f is the switching frequency and C is the snubber capacitance. This expression is valid as long as C is greater than the critical value. The critical value of the snubber capacitance is the value for which the device voltage just reaches the bus voltage at the end of tf.

The conduction losses are computed based on the assumption that the currents flowing through the device or its anti-parallel diode are linear. This is a fair assumption for high frequency transformers, since the dominant parameter is the leakage inductance. The average current through each device and diode are first derived and multiplied

by their respective on-state voltages to give the conduction loss. Since the derivation is straightforward, it will not be outlined here. However, for instance, the expressions for the device and diode conduction losses on the input bridge for Topology B, are evaluated as,

$$P_{con} \text{ / device} = 0.5 \text{ f } V_T \left[|I_\phi| (\tfrac{1}{2f} - t_o) + |I_\pi| (\tfrac{1}{2f} - t_\phi) \right] \quad ...(2.3.2a)$$

$$P_{con} \text{ / diode} = 0.5 \text{ f } V_D \text{ } |I_\pi| (t_o - t_f) \quad\quad ...(2.3.2b)$$

where, V_T, V_D are the on-state voltages of the device and diode respectively, I_ϕ, I_π, t_o, t_ϕ are as shown in Figure 2.3.2.

Table 2.3.1 summarizes the total switching and conduction loss figures for both the topologies A and B at the rated output power of 50kW while switching at 50kHz. These figures correspond to the design points selected in Table 2.2.1 (for stress comparison) for each of the topologies. The device fall time, t_f, which is essentially the tail time was selected as 0.5 μs and K as 0.25 from the manufacturer's data sheet [4]. V_T and V_D were selected as 3V and 1V respectively. For the computation of switching losses, the snubber capacitance was set to the critical value. This gives a very conservative estimate, since in practice the devices must be oversnubbed. The high conduction losses evident for all the topologies is a consequence of the device type. IGBTs have substantially higher on-state voltages than MOS-Controlled Thyristors (MCTs). With on-state voltages of 1.3V, assumed for the MCT [5], a 50% reduction in the conduction losses is realized for both the topologies. The switching losses for the MCTs have been computed assuming a turn-off switching behaviour which is similar to the IGBT.

Comparing the losses in Topologies A and B, the higher current stress in circuit A gives higher conduction and switching losses. The snubber capacitors are the smallest possible for ensuring that the device currents reach zero prior to an application of full voltage across the device.
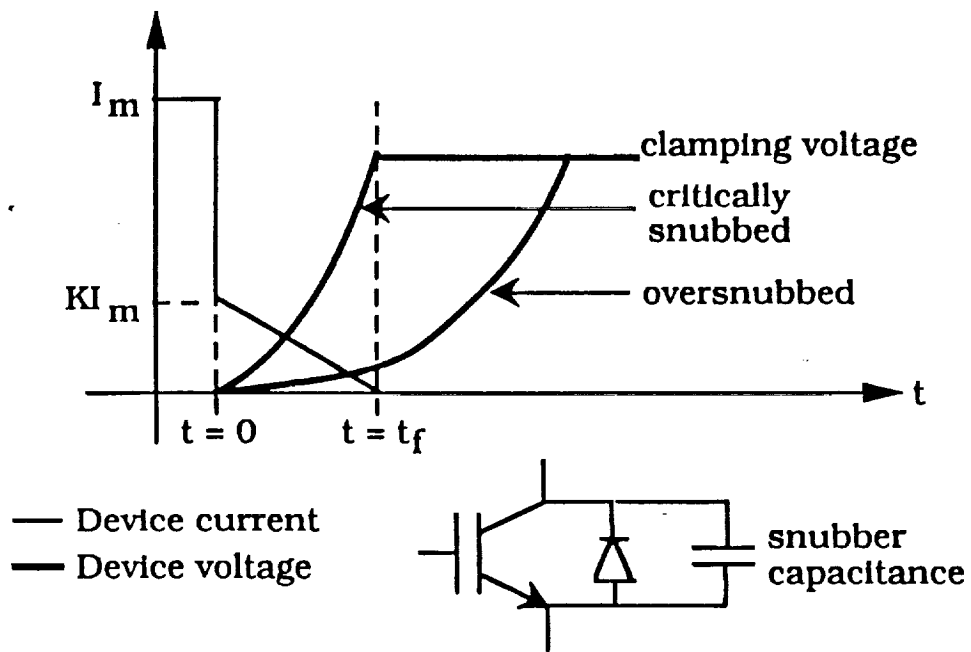
Figure 2.3.1   Typical model for the turn-off switching behaviour of an IGBT
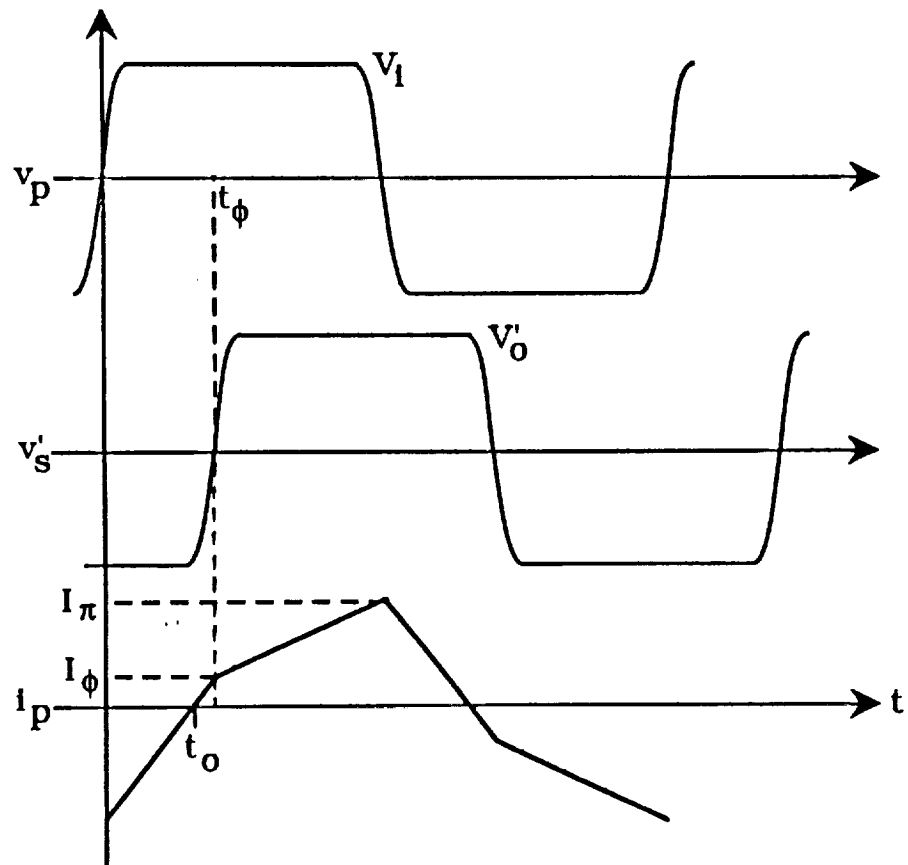
Figure 2.3.2   Operating waveforms for Topology B

TABLE 2.3.1

(Comparison of Projected Semiconductor Losses)

$(P_O = 50kW, V_1 = 200 \text{ Vdc}, V_O = 2000Vdc, f = 50kHz)$
$(IGBT: V_T = 3V, V_D = 1V, t_f = 0.5\mu s, K = 0.25)$
$(MCT: V_T = 1.3V, V_D = 1V, t_f = 0.5\mu s, K = 0.25)$

	Topology A		Topology B	
	IGBT	MCT	IGBT	MCT
Switching Losses(W)	668.8	668.8	257.6	257.6
Conduction Losses(W)	2273.9	1116.7	1684.7	801.2
Total(W)	2942.7	1785.5	1942.3	1058.8

2.4 Final Topology

Of the three proposed topologies, B and C possess the following desirable attributes :

1) Good range of control, especially for a dc conversion ratio(d) of unity.
2) Buck/boost operation possible.
3) High transformer utilization.
4) Low device and transformer stresses.
5) Bidirectional power flow.

However, bearing in mind the requirement of high power density, Topology C suffers in the following aspects :

1) Requires 4 additional devices(2 on each bridge), with its associated gate-driver circuits
2) Complex transformer construction, with a weight penalty associated with the additional yokes required for symmetry

Moreover, the additional devices in Topology C, imply additional switching events per cycle and hence a more complex controller.

On the other hand, Topology C shows a distinct advantage over Topology B, in its lower filter kVA-ratings. However, with the state-of-the-art multi-layer ceramic capacitors(MLC) available, which offer much higher power densities than conventional commutation-grade or electrolytic capacitors, the total weight required for the filter capacitors for Topology B is seen to be marginally higher than that for Topology C.

From a consideration of the above arguments Topology B seems to offer the most desirable characteristics. Further, from the analysis of device losses, it is seen that Topology B incurs the lowest losses at the optimum design point. Hence, on an overall basis, the most prudent selection for a converter topology would be B.

Also, since the control methodology for Topology A can also be incorporated in Topology B, a wider range of control is possible when their V_0' - I'_{oav} operating characteristics are superimposed, as shown in Figure 2.4.1. It should be remembered that the $\beta = \pi$ boundary for Topology A is identical to the diode bridge constraint for Topology B, hence they overlap. Now for instance, at higher load currents one could maintain tight control over this current as the output voltage is reduced, by essentially switching from Topology B mode of operation to Topology A mode as the overlapping boundaries for the two topologies is crossed. A significant implication of this is that the load current could be held constant even under short-circuit faults, and with all the devices always operating under soft-switching conditions.

2.5 Summary

In conclusion, considering the various desirable features of Topology B, it seems to be the most viable choice for a final topology. However, the high output voltage requirement (2000Vdc) seems to make the use of active output bridges difficult, as devices rated in the kilovolt range are limited in terms of switching speed. Also, the high power density needed mandates a high switching frequency. Thus, a modular approach is necessary for realizing high power at the high output voltages. For the specified output voltage, a series connection of two active half-bridges, as shown in Figure 2.5.1, is a possible solution. These aspects of circuit operation are currently under investigation and will be discussed in the final report.
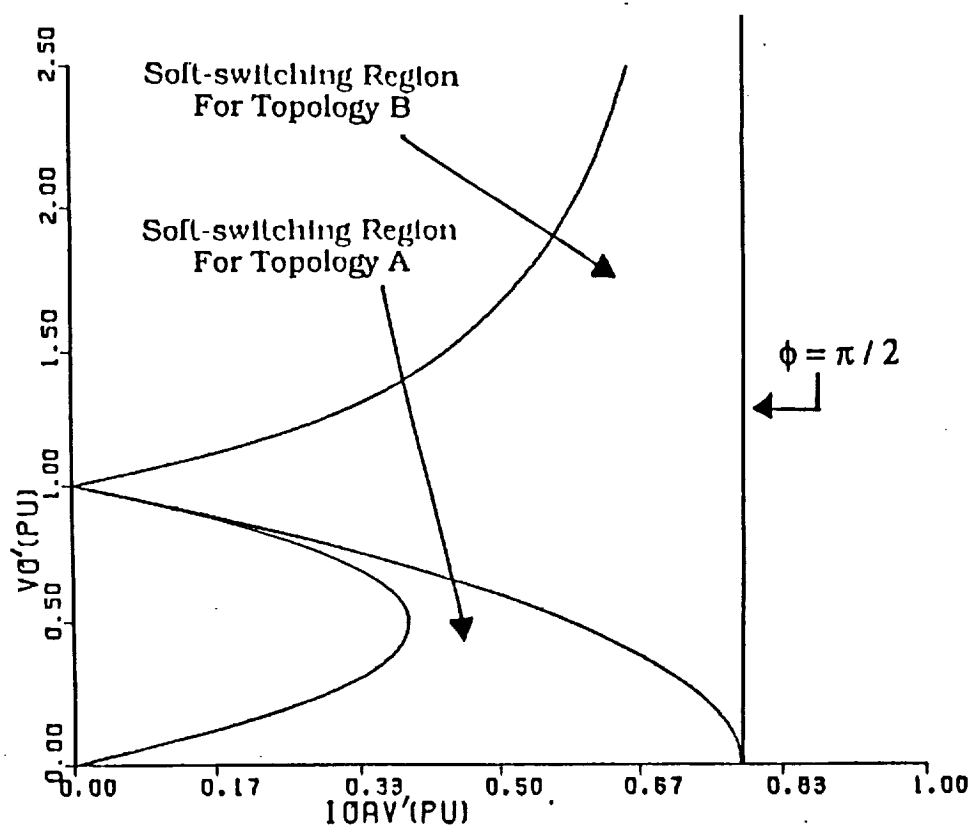
Figure 2.4.1   Superposition of the soft switching regions for Topologies A and B on the output voltage vs output current plane
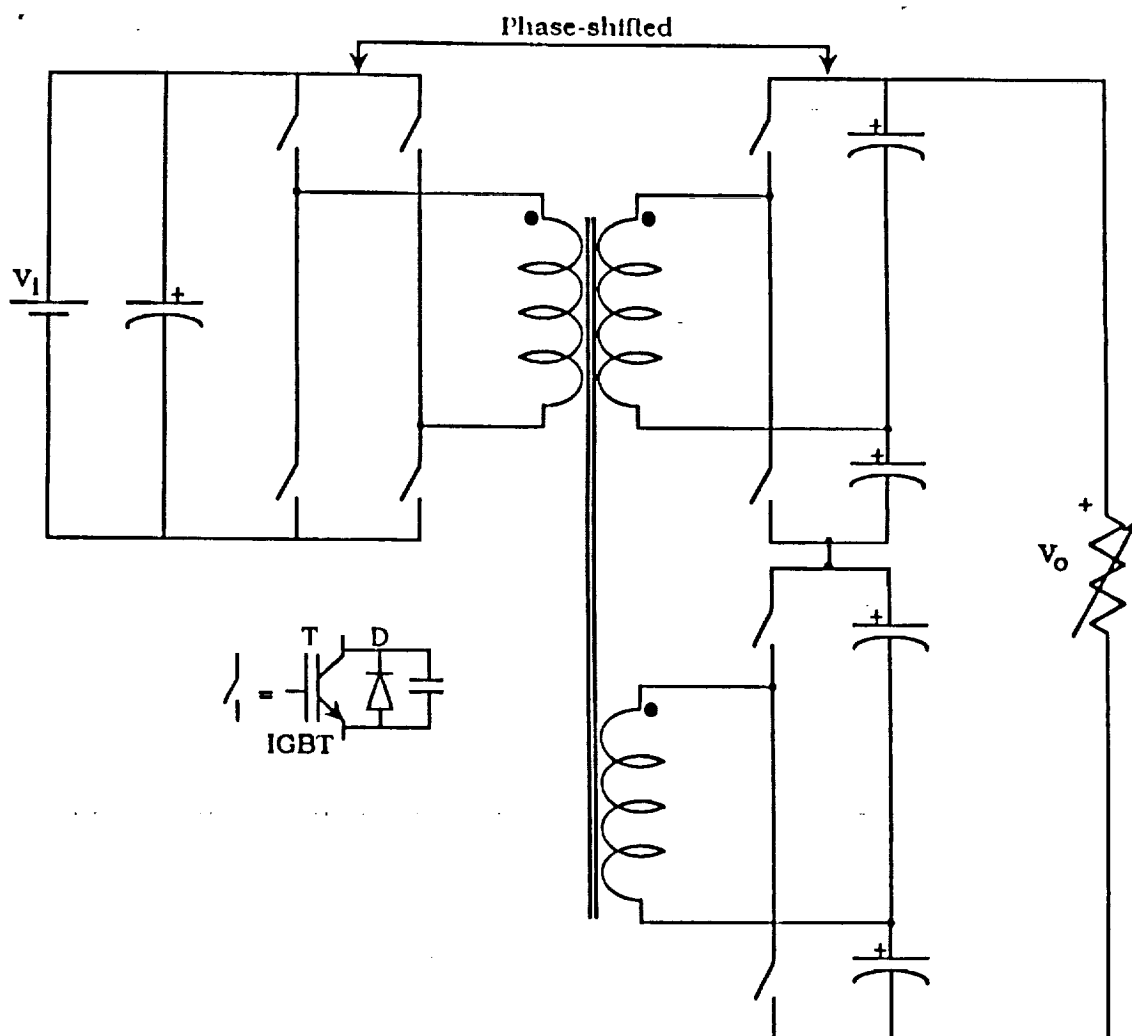
Figure 2.5.1   Schematic of Series Connected Single Phase Dual Active Bridges DC/DC Converter for High Voltage Outputs (Outputs are Half Bridges)

CHAPTER 3

CONSIDERATIONS ON THE SOFT SWITCHING REGION FOR TOPOLOGY B

3.1 Introduction

Having understood the operation of the proposed converter topologies from a simplified steady state analysis, it is now appropriate to relax some of the assumptions, in particular with regard to the transformer magnetizing inductance and snubber capacitance, and study their influence on the converter performance. The purpose of this exercise is to ascertain the change in the soft-switching region, if any. All the analysis will be carried out for the selected converter Topology B, only.

3.2 Effect of Finite Magnetizing Inductance of the Transformer on the Soft Switching Boundaries

For convenience, the circuit schematic of Topology B, the single phase dual active bridge dc/dc converter, is repeated in Figure 3.2.1a. Figure 3.2.1b shows the primary referred model for the converter, with the input and output bridges replaced by square wave voltage sources. The T-model has been assumed for the transformer, with half the leakage inductance shown on each side of the finite magnetizing inductance. It is valid to assume that the winding resistances are negligible compared to the leakage reactance at the high frequencies of interest.

Figure 3.2.2 shows the relevant operating waveforms for Topology B with the T-model for the transformer included, where ϕ is the controlled phase shift between the input and output bridges. Let the magnetizing inductance, L_m, be K*L, where L is the total leakage

20
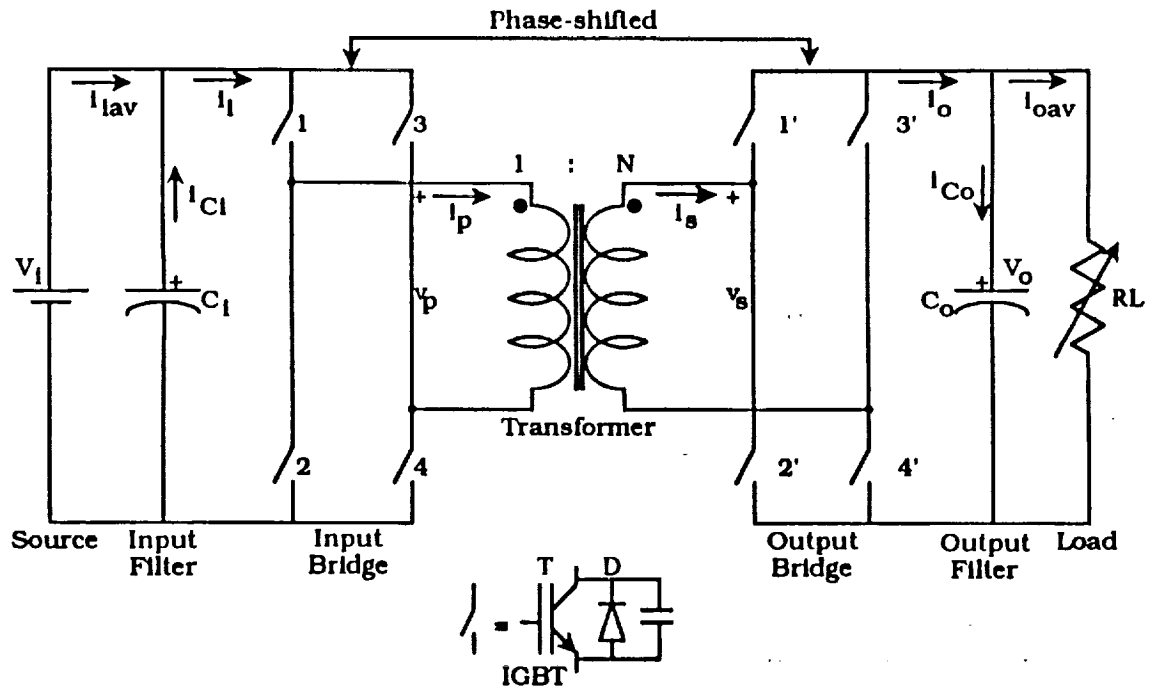
Figure 3.2.1a   Schematic of Single Phase Dual Active Bridges DC/DC
Converter (Topology B)
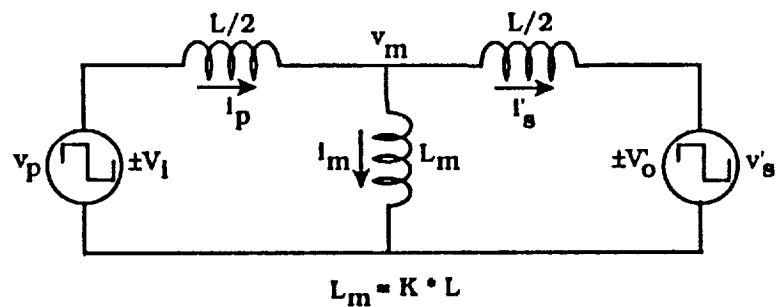
Figure 3.2.1b   Primary referred equivalent circuit of Topology B, with
T-model for the transformer
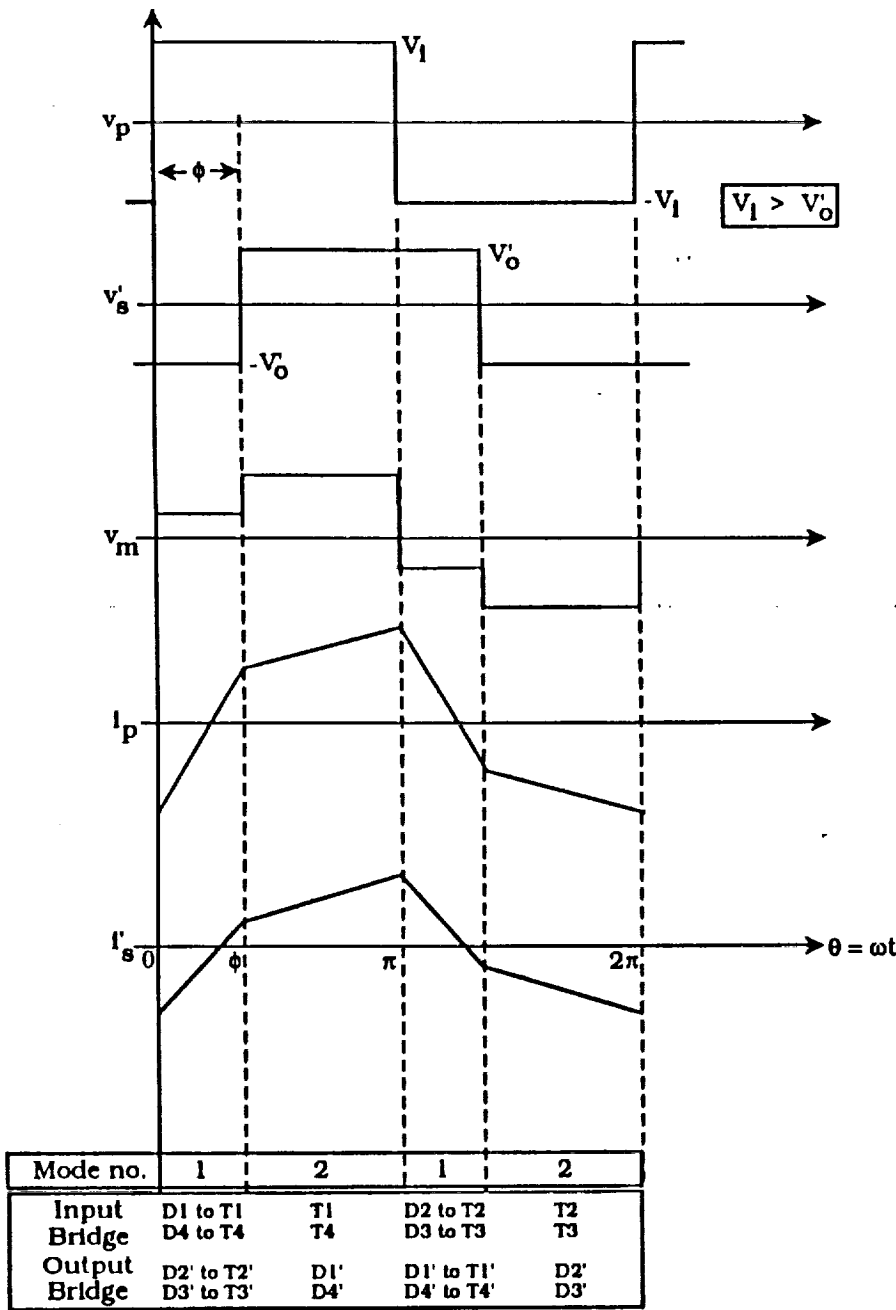
Figure 3.2.2 Idealized operating waveforms for Topology B, with T-model for the transformer

inductance and $K \geq 1$. Defining v_m as the voltage across L_m, we can then write i_p, i_s' and i_m as,

$$\frac{di_p}{d\theta} = \frac{v_p - v_m}{\frac{\omega L}{2}} \qquad \text{...(3.2.1)}$$

$$\frac{di_s'}{d\theta} = \frac{v_m - v_s'}{\frac{\omega L}{2}} \qquad \text{...(3.2.2)}$$

$$\frac{di_m}{d\theta} = \frac{v_m}{\omega L_m} \qquad \text{...(3.2.3)}$$

Note that v_p, v_s', v_m, i_p, i_s', i_m are functions of θ, where $\theta = \omega t$, and ω is the switching frequency in radians/sec.

Moreover,

$$i_m = i_p - i_s' \qquad \text{...(3.2.4)}$$

Eliminating i_m from Equations (3.2.1) to (3.2.4), we get,

$$\frac{di_p}{d\theta} = K_1 v_p - K_2 v_s' \qquad \text{...(3.2.5)}$$

$$\frac{di_s'}{d\theta} = K_2 v_p - K_1 v_s' \qquad \text{...(3.2.6)}$$

and,

$$v_m = \frac{1}{2 + \frac{1}{2K}}\left[v_p + v_s'\right] \qquad \qquad ...(3.2.7)$$

where,

$$K_1 = \frac{1 + \frac{1}{2K}}{\omega L(1 + \frac{1}{4K})} \qquad \qquad ...(3.2.8a)$$

and,

$$K_2 = \frac{1}{\omega L(1 + \frac{1}{4K})} \qquad \qquad ...(3.2.8b)$$

Again, two modes of operation can be identified for the converter. Evaluating the current i_p in each mode and using the half-wave symmetry conditions (as done in the ideal analysis), we get,

$$i_p(0) = -V_1 K_2\left[d\phi + \frac{\pi}{2}\left(\frac{K_1}{K_2} - d\right)\right] \qquad \qquad ...(3.2.9)$$

where,

$$d = \frac{V_o'}{V_i}$$

and, V_i is the input dc voltage, and V_o' is the primary referred output dc voltage.

Enforcing the soft-switching constraint for the devices on the input bridge, that is,

$$i_p(0) \leq 0$$

we get from Equation (3.2.9),

$$d \leq \frac{K_1}{K_2}\left[\frac{\pi}{\pi - 2\phi}\right] \qquad 0 \leq \phi \leq \frac{\pi}{2} \qquad \qquad ...(3.2.10)$$

Similarly, carrying out the modal analysis for i_s', and enforcing the soft-switching constraint for the output bridge,

$$i_s'(\phi) \geq 0$$

we get,

$$d \geq \frac{K_2}{K_1}\left[1 - \frac{2\phi}{\pi}\right] \qquad 0 \leq \phi \leq \frac{\pi}{2} \qquad \qquad ...(3.2.11)$$

Note, as L_m tends to infinity(i.e. K tends to infinity). Equations (3.2.10) and (3.2.11) reduce to Equations (3.3.7)[??] & (3.3.8)[??] respectively.

The average output current, i_{oav}', can be evaluated by taking the average of the product of i_s' and the output bridge switching function. This turns out to be,

$$i_{oav}' = V_1 \phi K_2\left[1 - \frac{\phi}{\pi}\right] \qquad \qquad ...(3.2.12)$$

Hence, the output power, P_o, is given as,

$$P_o = V_o' i_{oav}'$$

$$= \frac{V_1^2}{\omega L} d\phi\left[1 - \frac{\phi}{\pi}\right]\left[\frac{1}{1 + \frac{1}{4K}}\right] \qquad \qquad ...(3.2.13)$$

Note, as K tends to infinity, P_o reduces to the idealized output power expression shown in Equation (3.3.10) [1].

To illustrate the influence of the magnetizing inductance, the output power as derived in Equation (3.2.13) is plotted as a function of ϕ, for two values of K, with d set to unity. Figure 3.2.3 shows this plot with the soft-switching boundaries also evaluated for the same values of K. The soft-switching boundaries are given in Equations (3.2.10) and (3.2.11). $K = 10^5$ represents a large value of the magnetizing inductance. $K = 1$, although not realistic, represents the other extreme for the magnetizing inductance. As K increases the soft-switching boundaries come closer, thus shrinking the desired region of soft-switching. This is seen to be reasonable, because as the magnetizing inductance decreases, in effect the load appears more lagging, which, as stated earlier, is a precondition for soft switching. Also, for the case $d = 1$, the power transferred to the output decreases with decrease in K. The penalty for lower magnetizing inductance is thus, evidently, low transformer utilization.

Figure 3.2.4 shows the soft-switching region on the V_o'- i_{oav}' plane for the same two values of K. It is seen that for low values of the output current, the region of soft-switching widens as K decreases. However, the maximum i_{oav}', governed by the $\phi = \pi/2$ boundary (explained in Chapter 3 of Reference 1), diminishes with decreasing K. The parameter K allows a mechanism for trading of range over d achievable under soft switching.
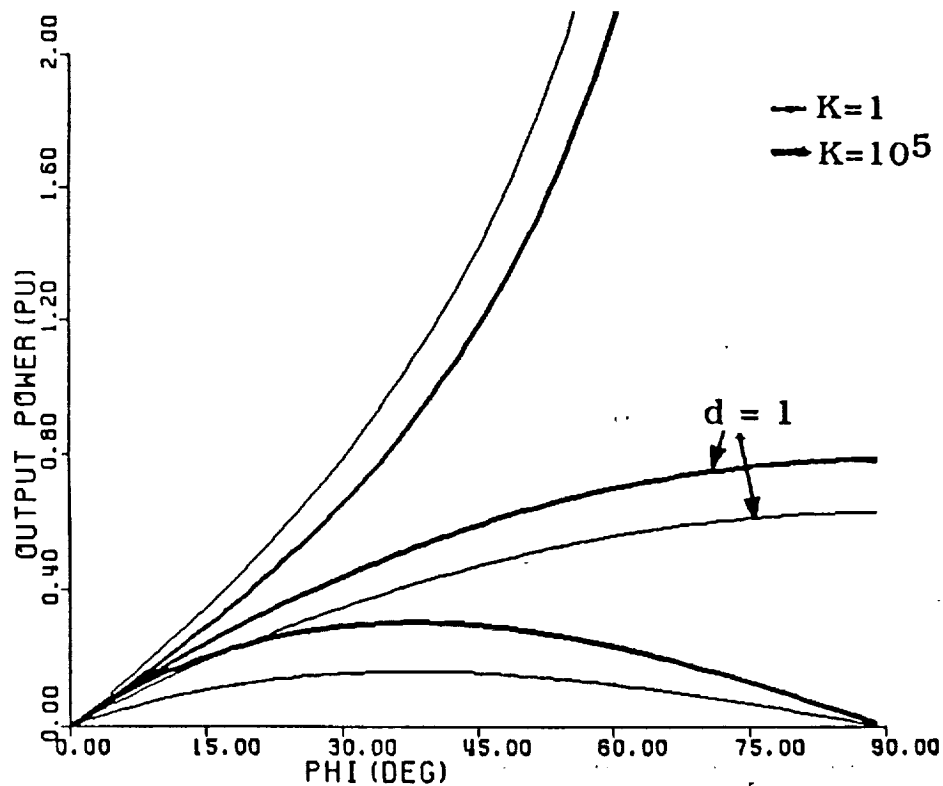
Figure 3.2.3   Effect of K = L_m/L on the output power vs phase-shift
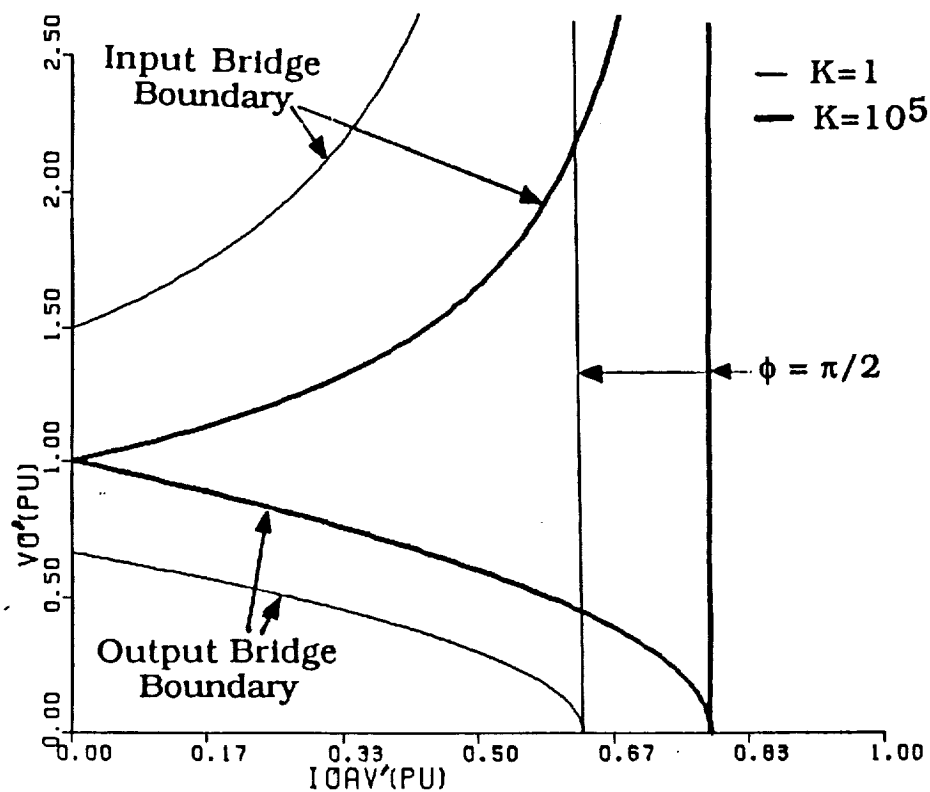for the d=1 and soft switching boundary curves

Figure 3.2.4   Effect of K on the soft switching region shown on the
output voltage vs output current plane

3.3   Effect of Snubber Capacitance on the Soft Switching Boundaries

The purpose of this section is to study the influence of snubber capacitance on the minimum current required in the leakage inductance of the transformer, during turn-off of any of the devices on either of the input or output bridges. The derivation of the soft-switching regions from the steady state analysis of the proposed topologies, in chapter three, was carried out under the assumption that the minimum current required is zero. Although; not a very realistic assumption, it was necessary to do so, to ascertain the fundamental working principle of the proposed converters from a simplified analysis. It is shown here that with increasing values of snubber capacitance, the minimum current required for zero voltage switching of any of the devices increases. This would further restrict the region available for soft-switching on the output voltage versus output current plane.

Figure 3.3.1a shows one pole of the input bridge. L represents the leakage inductance of the transformer. C1 and C2 are the snubber capacitances for the input bridge devices, T1 and T2. Note, C1 = C2 = C. The effect of snubber capacitance on the minimum current required through L, for zero-voltage switching on the input devices will only be considered. Let us assume that at t = 0, the device T1 turns-off, as shown in Figure 3.3.1b. All other devices, shown in Figure 3.3.1a are not conducting at this instant of time. The turn-off time of the device will be considered negligible, and the value of C1 (or, C2) sufficiently large to ensure very little change in the voltage across T1 during its turn-off interval. Once the device turns off, the inductor current resonates through the parallel combination of C1 and C2. The current, I_p, flows through L in the direction shown in Figure 3.3.1a. The output bridge is replaced by a primary-referred voltage source, V_o', with the proper polarity. We need to find the minimum inductor current required at t = 0, which ensures that the voltage across T1 reaches the clamping value (V_i) when I_p reaches zero. Let t = t_m be the instant of time at which I_p resonates to zero. Hence,
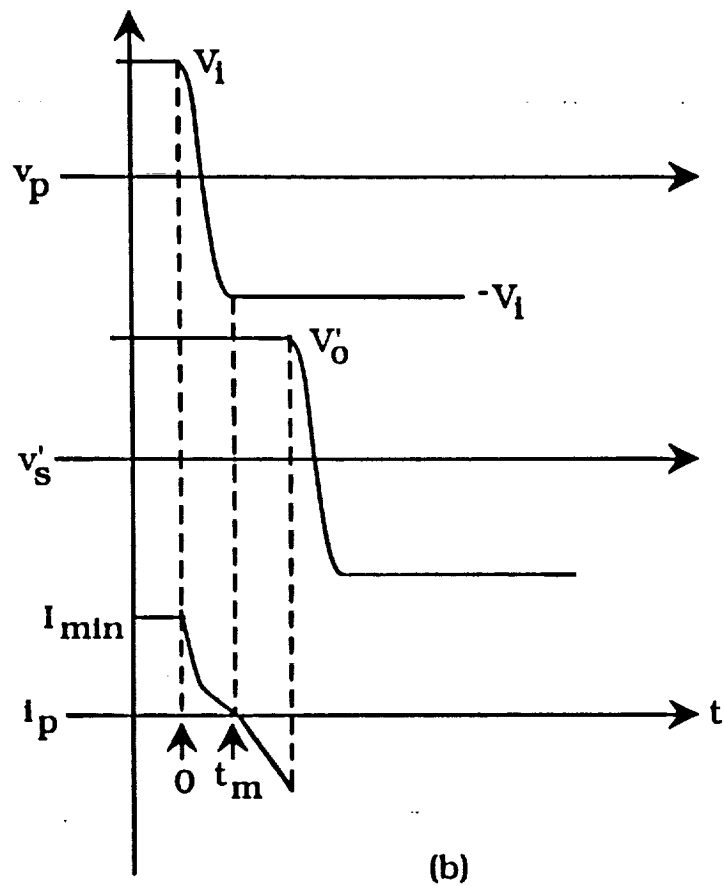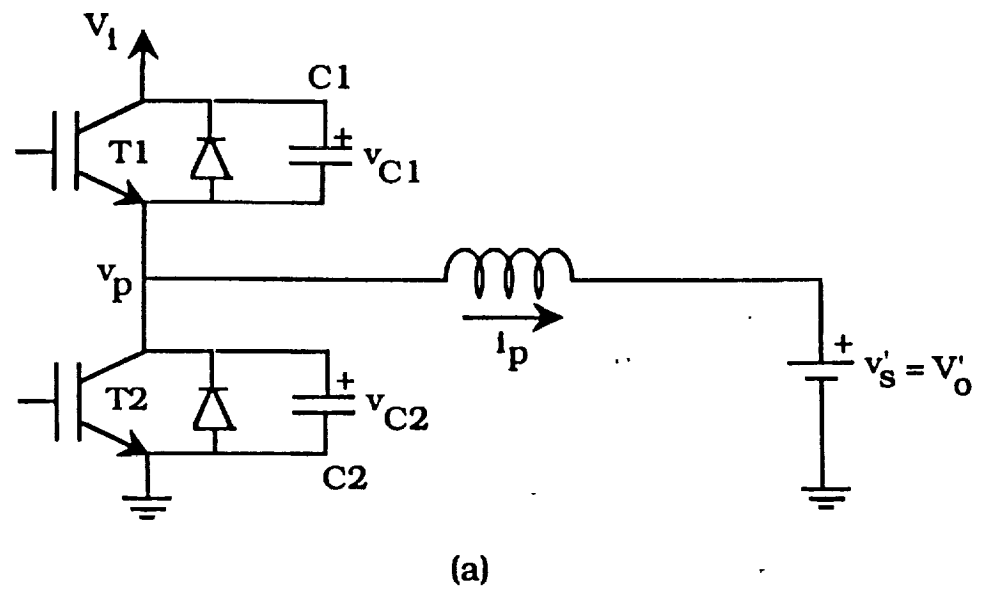
Figure 3.3.1   (a) One resonant pole of the input bridge (Topology B) (b) Minimum inductor current required at instant of turn-off of T1, to resonate the pole voltage from $+V_l$ to $-V_l$

at t = 0,

$$i_p = I_{min}$$
$$v_{C1} = 0$$
$$v_{C2} = V_1$$

and, at t = t_m

$$i_p = 0$$
$$v_{C1} = V_1$$
$$v_{C2} = 0$$

During, the interval $0 \leq t \leq t_m$,

$$i_p = C1 \frac{dv_{C1}}{dt} + C2 \frac{dv_{C2}}{dt} \qquad ...(3.3.1)$$

Since, C1 = C2 = C

$$\frac{dv_{C1}}{dt} = \frac{dv_{C2}}{dt} = \frac{dv_C}{dt}(say) \qquad ...(3.3.2)$$

Hence, from Equations (3.3.1) and (3.3.2), we get,

$$i_p = 2C \frac{dv_C}{dt} \qquad during \ 0 \leq t \leq t_m \qquad ...(3.3.3)$$

From, Energy Balance considerations,

$$E_{(t = 0)} = E_{(t = t_m)} + E_{loss} + E_{delivered}$$

Assuming, lossless circuit elements, we get,

$$\frac{1}{2} L I_{min}^2 + \frac{1}{2} C2 V_1^2 = \frac{1}{2} C1 V_1^2 + E_{delivered} \qquad ...(3.3.4)$$
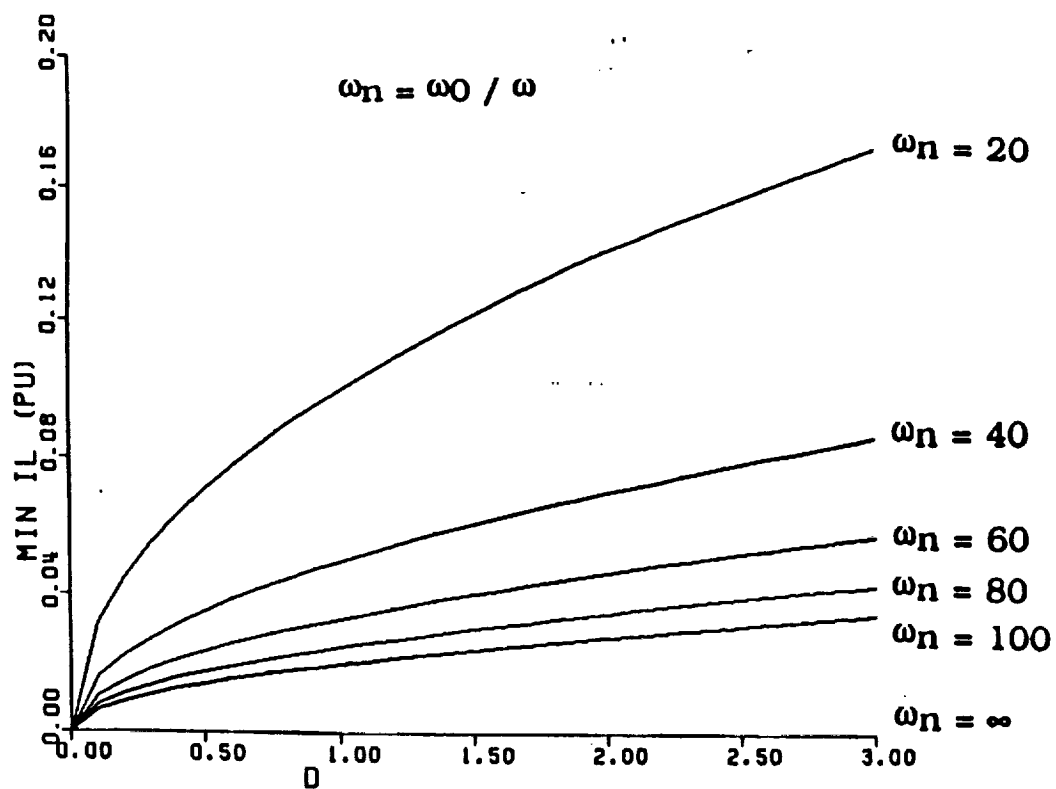
Figure 3.3.2 Required minimum inductor current vs d with ω_n as the parameter

C increases. Also, for a fixed value of L, ω and C, I_{min} increases as d increases.

It can be seen that as C is increased, switching losses decrease. However, the minimum current requirement imposed by Equation (3.3.7) restricts the Output voltage-Output current plane that can be reached under soft switching conditions. Consequently, this becomes an important limit and needs to be explored further in detail, incorporating the simultaneous influence of the snubber capacitance on the output bridge devices, which has been ignored here. It should be noted that the decrease in VA-plane due to C is compensated, atleast in part, by the impact of the transformer magnetizing inductance.

CHAPTER 4

DESIGN CONSIDERATIONS FOR HIGH POWER, HIGH FREQUENCY TRANSFORMERS

4.1   Introduction

The transformer, a necessary element in any high power dc/dc converter for galvanic isolation, is by far the dominant component in determining converter power density. High power density requirements of 0.2 - 0.3kg/kW with voltage outputs in the order of kilovolts coupled with the low leakage requirement, calls for a rigorous design methodology. At the very outset, the need for high operating frequencies to achieve the desired power density becomes evident.

Broadly speaking, the two fundamental issues in the design of any high-power high-frequency transformer are minimum losses and low leakage inductance. The two loss components associated with the transformer, namely core and copper losses, are strongly related to the frequency. Core loss, for a given frequency and flux density, is material dependent. Consequently, as a first step in the design process, an investigation of various high frequency core materials is essential. Copper loss in the transformer is extremely sensitive to the leakage flux distribution in the window region, which in turn is dependent on the core and winding geometry. A major focus of this chapter is on the influence of different winding arrangements on the winding losses and leakage inductance.

As mentioned earlier, in the proposed dc/dc converter, the presence of a certain amount of leakage inductance (governed by the rated power, frequency and design point) is crucial to the operation of the converter, since it functions as the main energy transfer element from one dc voltage source to the other. On the other hand, too high a value restricts maximum power transfer. In essence, the leakage inductance needs to be carefully controlled. This design objective is a

34

relatively difficult task to meet in conventional transformers. Coaxial windings, used primarily for very high frequency (radio frequency range) transformers, seem to offer an interesting and viable option. The latter part of this chapter addresses such winding techniques.

4.2 Core selection

The characteristics of a good core material include low specific core losses (defined as losses per unit volume or per unit mass) at high operating frequencies, high saturation flux density, high power/weight ratio, and good thermal and mechanical properties. In the light of these characteristics, three candidates, Ferrite PC40 Permalloy80(0.5mil) and Metglas2605SC(1mil) were investigated. Table 4.2.1 lists some of their salient properties.

To characterize these core materials, the specific core losses were measured for different frequencies over a wide range of flux densities under square wave voltage excitation. These tests were carried out owing to the unavailability of such data for square wave excitation. A half-bridge inverter, using Power MOSFETs as switches, was fabricated to generate the square wave voltage across a 4-turn foil-wound coil mounted on the core under test. The core loss was measured by integrating the product of the voltage and current on the coil on the LeCroy 9400 digital oscilloscope. The core loss figure includes the winding losses, which were estimated to be small enough (within 1%) to be neglected without much error. Figures 4.2.1a, b, c & d show specific core losses (measured as mW/cc) plotted as a function of the flux density on a log-log scale for the three candidate materials at 10, 25, 50 and 100kHz respectively.

It is seen that Metglas exhibits the highest core losses for all the test frequencies over the entire range of test flux densities, and is hence not considered to be a viable core material for our application, given the high power density and high efficiency constraints. The Permalloy80(0.5 mil) material appears to be the most promising of the

TABLE 4.2.1

(Test Core Material Properties)

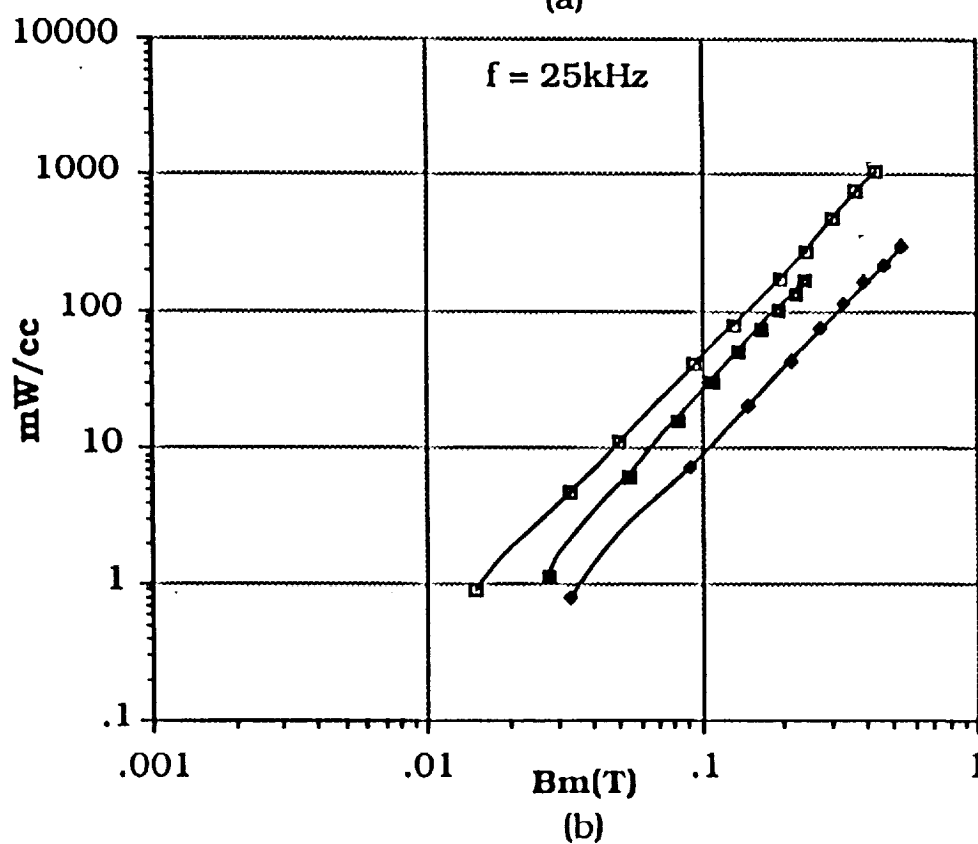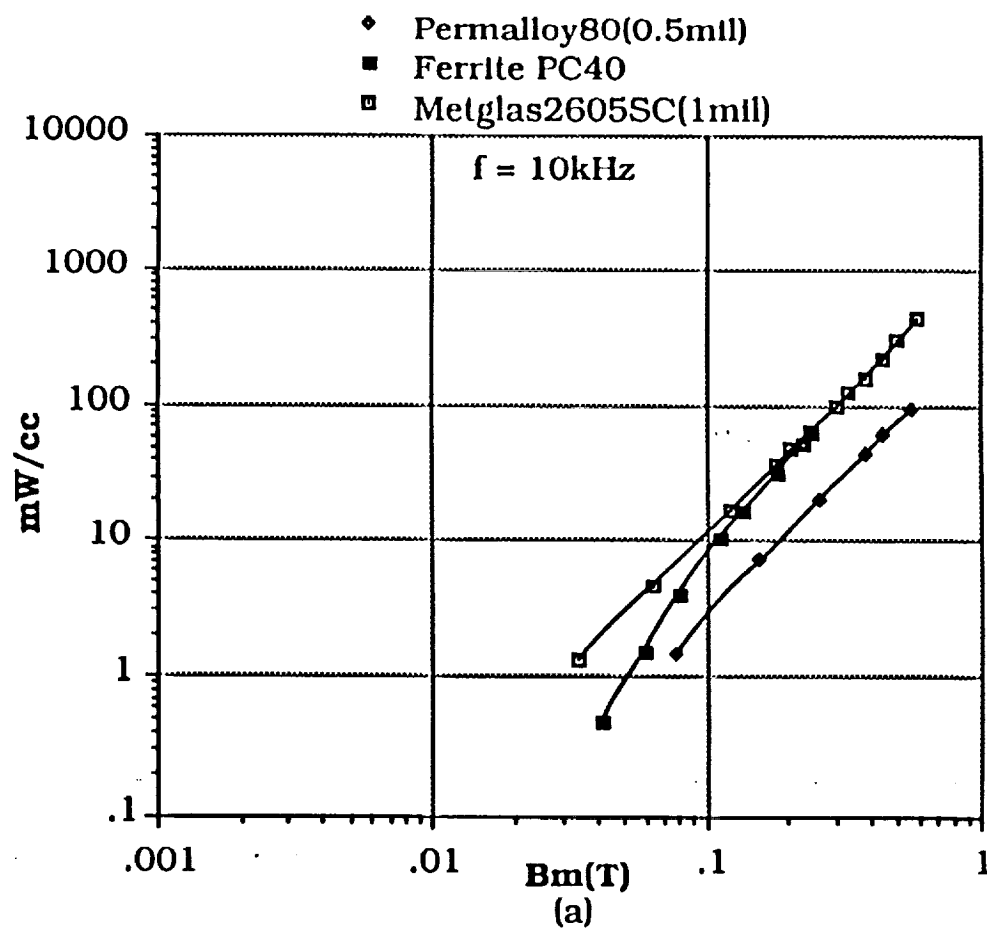|	Ferrite(PC40)	Permalloy80	Metglas2605SC
Type	Cerramic	Tape-wound	Tape-wound (Amorphous)
Composition	Fe_2O_3 50% MnO 50%	Ni 80% Fe 16% Mo 4%	Fe 81% B 13.5% Si 3.5%, C 2%
Bm(T)	0.2	0.5	0.75
μ	2300	30000	50000
Resistivity(Ω-m)	6.5	0.57	1.25
Density(gm/cc)	4.8	8.7	7.3
Shape	Wide range- E,I,U,Toroids, Pot, etc.	Toroids, Cut C-cores	Toroids, Cut C-cores

Figure 4.2.1   Specific core loss vs peak flux density for the three
candidate materials at (a) f = 10 kHz, (b) f = 25 kHz
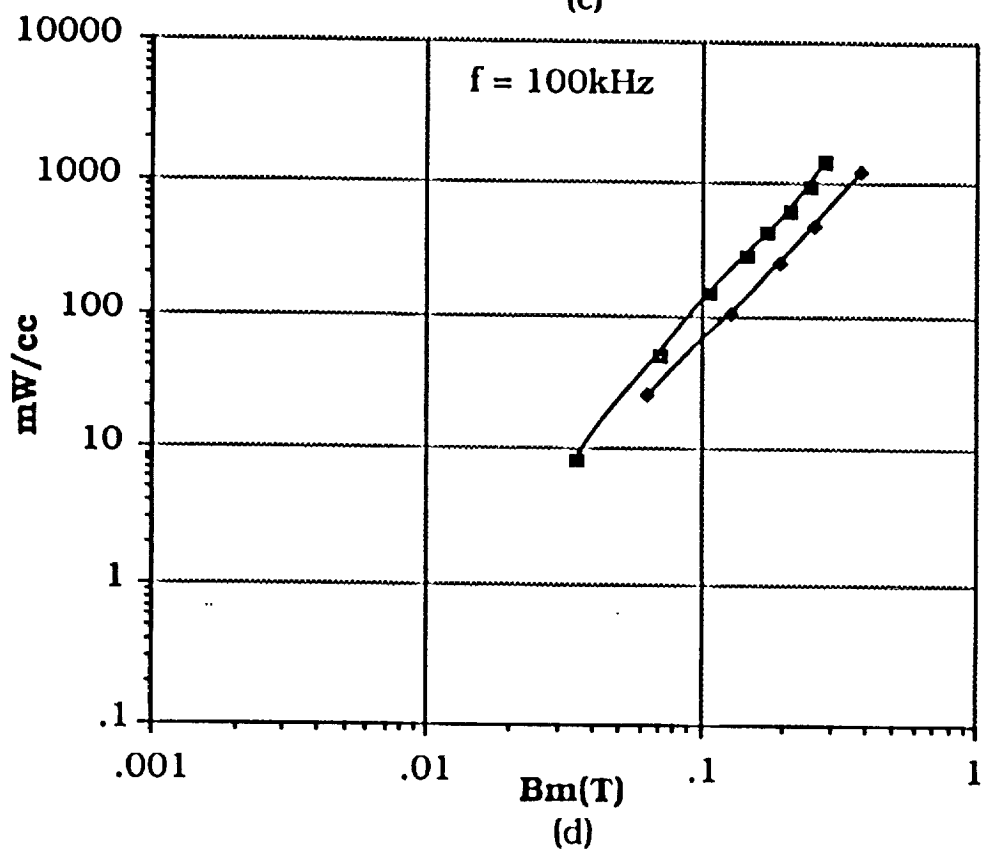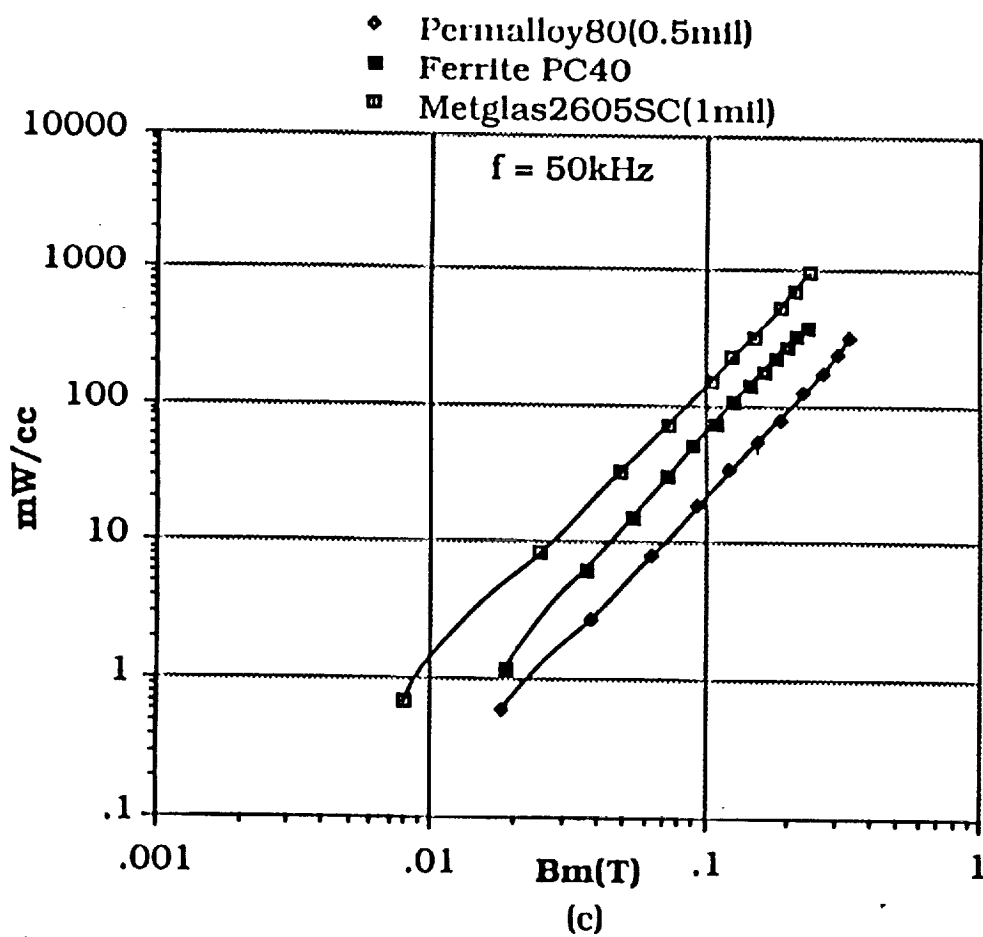
Figure 4.2.1 Specific core loss vs peak flux density for the three candidate materials at (a) f = 50 kHz, (b) f = 100 kHz

three materials for all the test frequencies. On the other hand, even though the Ferrite material has higher losses than the Permalloy80, the former offers a wide range of core geometries. In particular, for high power, low leakage transformer designs, the shell-type of transformer built from E-E cores is the most desirable. Such core shapes are readily available in the Ferrite material. Moreover, there is a distinct cost advantage in going for Ferrite cores.

To achieve power levels in the megawatt range, which is the ultimate goal, a modular approach must be adopted, where multiple identically rated modules can be paralleled. To demonstrate this concept, two 50kW units will be fabricated and operated in parallel. One of the transformers will be constructed from Ferrite E-E cores and the other from Permalloy80 toroidal cores, in order to obtain detailed comparison of the two core materials.

Having laid the foundation for studying core losses, it is now important to look at the copper losses. The following sections involve a study of two possible winding arrangements, conventional and coaxial. Various interleaving arrangements of winding sections would fall under the category of conventional windings.

4.3 Conventional Winding Arrangements

The primary objective of this section is to study the influence of the various conventional winding geometries on the copper losses. Copper losses in a high frequency transformer are predominantly due to skin and proximity effects, which are collectively called eddy current effects.

Skin effect associated with a conductor carrying alternating current, is the redistribution of the current towards the surface due to the magnetic field generated by this current. The resultant increase in the current density can be seen, from a circuit viewpoint, as an increase in the effective resistance of the conductor. Consequently, for a given current the I^2R losses would increase. This phenomenon is

strongly related to the frequency. Proximity effect is the phenomenon in which circulating eddy currents are induced in the conductor by time-varying magnetic fields generated from nearby current carrying conductors. These eddy currents generate extra losses and are also strongly related to the frequency and magnitude of the external field.

The two losses can be expressed as,

$$P_{skin} = F * I^2 \qquad \qquad ...(4.3.1)$$

$$P_{prox} = G * H^2 \qquad \qquad ...(4.3.2)$$

where,   F is the effective resistance due to skin effect of the
conductor
G is the proximity effect factor
I is the current in the conductor, and
H is the external magnetic field caused by surrounding currents.

F and G are functions of frequency, conductor type (foil, litz wire, or solid round wire), dimensions and material.

Minimization of winding losses, due to the eddy current effects, in high frequency transformers is a fairly challenging task and involves, firstly, the selection of the proper conductor type and dimensions and secondly, an understanding of the influence of the winding geometry on the leakage (or, stray) field distribution in the window region. It is important to calculate this leakage field to assess the proximity effect winding losses.

To appreciate the influence of the conductor type on the effective resistance due to skin effect, for instance, three standard conductor types, viz. foil, litz wire and solid round wire were considered. For each conductor type the cross-sectional area was kept constant, to keep the dc resistance/unit length, R_{dc}, fixed. The

effective resistance due to skin effect for each conductor type is given from [6,7,8] as,

$$F_{strip} = \frac{R_{dc}\,\gamma}{2}\left[\frac{\sinh\gamma + \sin\gamma}{\cosh\gamma - \cos\gamma}\right] \quad \Omega/m$$

...(4.3.3a)

where, $\gamma = \dfrac{h}{\delta}$

$$R_{dc} = \frac{1}{h\,w\,\sigma} \quad \Omega/m$$

where,   h = foil thickness
w = foil width
σ = electrical conductivity
δ = skin depth = $\dfrac{1}{\sqrt{f\,\pi\,\sigma\,\mu_0}}$
μ_0 = absolute permeability
f = frequency

$$F_{round} = \frac{R_{dc}\,\gamma}{2}\left[\frac{ber(\gamma)\,bei'(\gamma) - bei(\gamma)\,ber'(\gamma)}{ber'^2(\gamma) + bei'^2(\gamma)}\right] \quad \Omega/m$$

...(4.3.3b)

where,   ber(.), bei(.) and bei'(.) are the Kelvin functions,

$$\gamma = \frac{d}{\delta\sqrt{2}}$$

$$R_{dc} = \frac{4}{\pi\,\sigma\,d^2} \quad \Omega/m$$

where,   d = diameter of round wire

$$F_{litz} = \frac{F_{strand}}{N} = \frac{N \, R_{dc} \, \gamma}{2} \left[\frac{ber(\gamma) \, bei'(\gamma) - bei(\gamma) \, ber'(\gamma)}{ber'^2(\gamma) + bei'^2(\gamma)} \right] \quad \Omega/m$$

...(4.3.3c)

where, $\quad \gamma = \dfrac{d_{strand}}{\delta\sqrt{2}}$

$$R_{dc} = \frac{4}{\pi \, \sigma \, N \, d_{strand}^2} \quad \Omega/m$$

where, $\quad$ d_{strand} = litz strand diameter

N = number of litz strands

assumption : $\quad$ negligible thickness of enamel on each strand

A standard litz wire was selected, consisting of 329 strands and a total cross-sectional area of 16585cmils (1cmil = $\pi/4$mil^2, where, 1mil = 25.4 * 10^{-6}m). Keeping this as the common cross-sectional area, and choosing f = 50kHz, the effective resistance for each conductor type, as given by Equations (4.3.3a, b, c), was computed. The thickness of the foil was selected as 2δ, where δ ~ 12mils at f = 50kHz (for copper). Table 4.3.2 summarizes the effective resistance for each conductor type based on the above considerations. As expected the solid round conductor shows the highest increase in effective resistance, and is certainly not suitable as a conductor type for high frequency applications. Foil and litz wire show very little change in their effective resistances from the dc value. Of course, as foil thickness is increased its effective resistance goes up. The choice between the two conductor types, for high frequency transformer applications, is thus dependent on various design trade-offs including relative window dimensions, window fill factor, number of turns, etc.

As a first consideration, the choice of core geometry is dictated

TABLE 4.3.2

(Effective Resistance due to Skin Effect for the three conductor types)

(f = 50kHz, $\delta \sim$ 12mils)

	R_{dc} (Ω/m)	F (Ω/m)	% Change
Foil (thickness = 2δ)	2.0229	2.2571	11.6%
Solid Round	2.0229	6.1756	205.3%
Litz (329 strands)	2.0229	2.0233	0.02%

by the low leakage inductance desired, and also, the winding arrangement. The use of shell-type core for conventional transformers, made from E-E cores, is seen to be desirable. This, in turn, leaves us with Ferrite as the core material of choice (for reasons mentioned in the last section). Other attractive geometries such as pot-cores, are not available for the high power levels of interest.

To address the issue of the influence of winding geometry on leakage flux distribution, three typical conventional winding arrangements, labelled X, Y and Z, shown in Figure 4.3.1 were studied. Arrangement X consists of one primary and one secondary winding wound concentrically on the centerpost of a shell-core. Arrangement Y consists of one secondary winding sandwiched between two primary windings, which are connected in parallel. All the winding sections are wound concentric to the centerpost. Arrangement Z consists of the same winding sections as in Y, with the sections now stacked vertically, concentric to the centerpost. The two primary sections are connected in parallel. To analyze the copper losses, the transformer, for each winding arrangement, was designed for the actual specifications, viz, 50kW, 50kHz, 200V primary and 2000V secondary, maintaining the same amount of copper. Due to the unavailability of a finite element eddy current solver package, the computation of these losses was done with the aid of a high frequency transformer design program [8].

This software referred to as "TID" (Transformer Inductor Design) by its author takes as inputs pertinent core, window and winding section dimensions. It also accounts for the conductor type (foil, litz wire or round) with all its relevant dimensions. The Fourier components of the current flowing in each winding must also be specified. It then computes the total winding losses by calculating the skin effect and proximity effect losses separately for each frequency component and simply adding all the terms together. The loss due to skin effect is computed as given in Equation(4.3.1). As seen from the proximity effect Equation (4.3.2), the field distribution in the window region must first be calculated. This is done using the method of
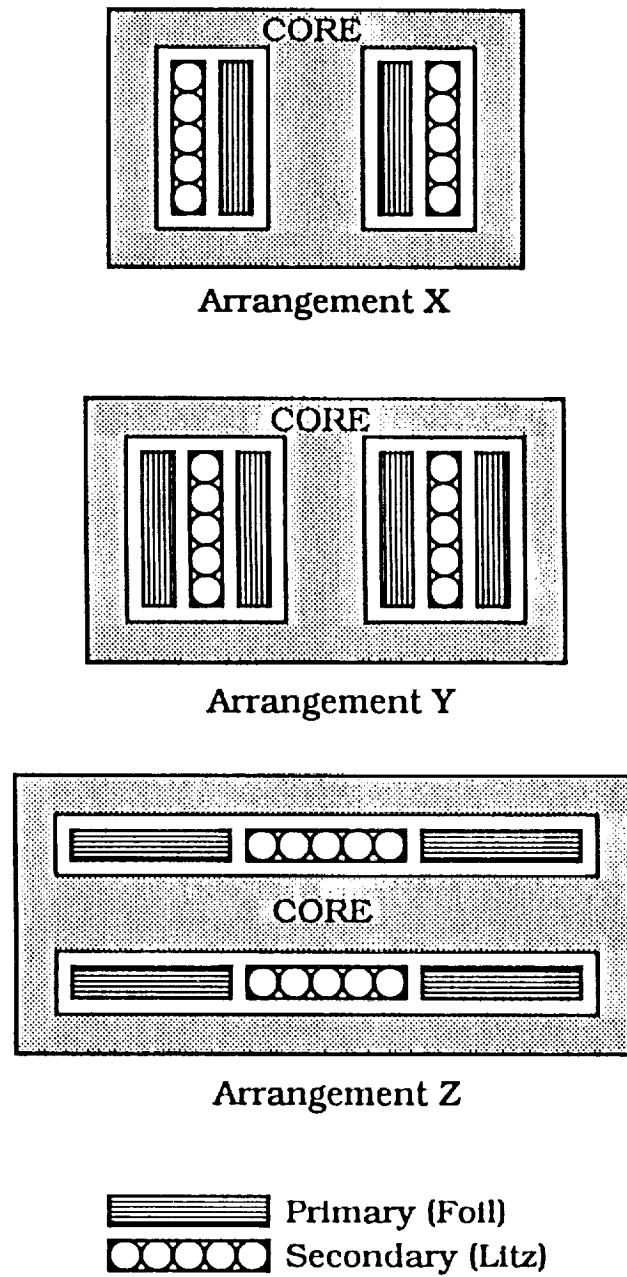
Arrangement X

Arrangement Y

Arrangement Z

Primary (Foil)
Secondary (Litz)

Figure 4.3.1   Three conventional transformer winding arrangements X, Y, Z

images, which in essence consists of replacing the effects of a boundary on an applied field by simple distributions of currents behind the boundary line, the desired field being given by the sum of the applied and the image fields [9].

Setting the maximum operating flux density at 0.2T, typical for the selected Ferrite material, the required core cross-sectional area can be calculated from the transformer voltage relation, given below,

$$V_{primary} = 4 * N_{primary} * B_{max} * f * A_c \qquad ...(4.3.4)$$

where, $N_{primary}$ is the number of primary turns, f is the frequency of operation and A_c is the core cross-sectional area. Note, since the excitation voltage is square-wave, the form factor is set to 4. At this point, however, the number of primary turns is also not known. Considering the high levels of primary current and the high turns ratio required, $N_{primary}$ was set to 3. Moreover, to maintain a reasonably high fill factor, and given the constraint of providing sufficient insulation at the high voltage levels, a foil-type of primary conductor was selected. The core cross-sectional area can now be determined from Equation (4.3.4), and further the core centerpost dimensions can be fixed.

The primary foil thickness was set to approximately 2δ, where δ is the skin-depth (at 50kHz). The conductor type for the secondary winding, consisting of 15 turns, was selected as litz wire. To determine the amount of copper area, the current density and operating rms current at full power must be known. The current density was selected as 500 cmil/A. To ascertain the rated current, a reasonable design point was selected from the transformer kVA versus output power characteristics for Topology B, shown in Figure 4.3.2. On the d = 1 (corresponding to equal primary and secondary voltages referred to primary side) curve, the design point was chosen so that the transformer utilization, defined as ratio of output power to
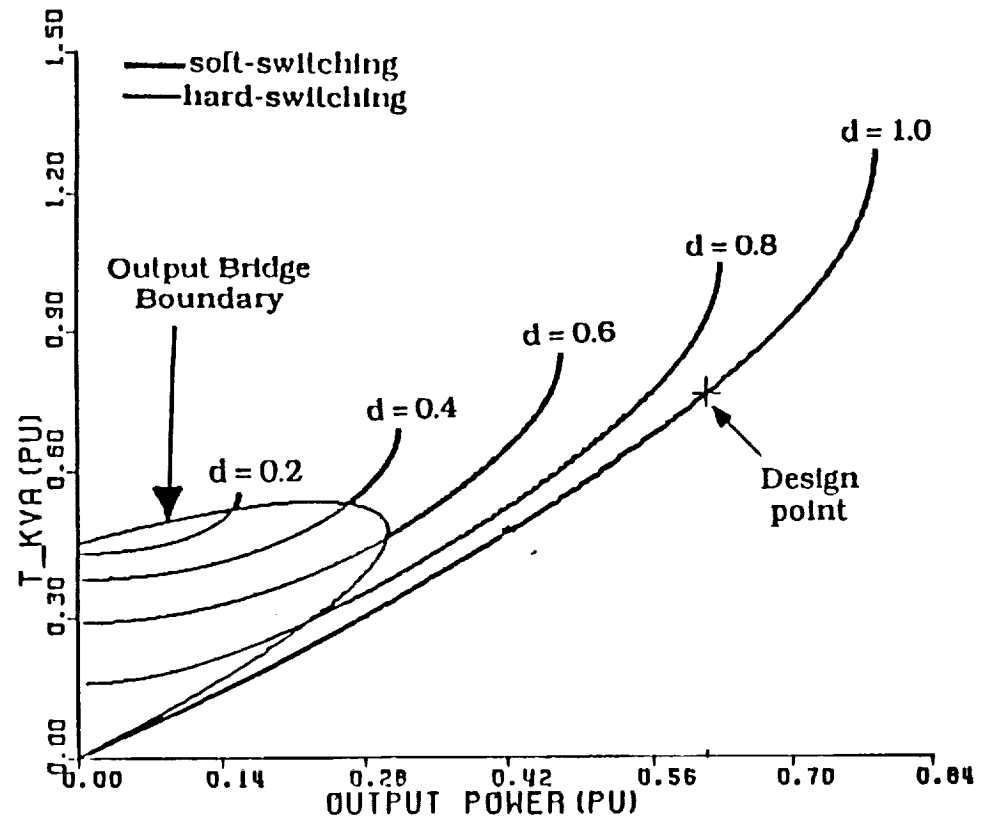
Figure 4.3.2 Transformer-kVA vs output power for Topology B, showing design point

transformer kVA, would be fairly high. The normalized output power for Topology B is given as,

$$P_O = d\, \phi\, (1 - \frac{\phi}{\pi})\qquad ...(4.3.5)$$

where, d is the dc conversion ratio, referred to the primary side, and ϕ is the controlled phase-shift between the the input and output bridges. The selected design point corresponds to $P_O = 0.63$ (normalized). Substituting this in Equation (4.3.5) and setting d = 1, gives $\phi = 50.4$ degrees. Now, the normalized selected design point must correspond to the rated output power of 50kW. The power base is given as,

$$P_b = \frac{V_1^2}{\omega L}$$

Hence,

$$0.63 * P_b = 50kW$$

Putting, $V_1 = 200V$ and $\omega = 2\pi f$, we get,

$$L = 1.6\ \mu H$$

where L is the required transformer leakage inductance at f = 50kHz.

Further, knowing ϕ, d, L, f and V_1, the primary rated rms current then turns out to be 312 A, while the secondary rated rms current is 31.2 A. Knowing the rated current levels in each winding and the specified current density, the primary foil dimensions could be completely defined. For the secondary litz wire, an equivalent AWG of 6 was needed. Next, as required by the "TID" program the winding and window dimensions, and the Fourier series component of the

primary and secondary current at the design point were calculated. Appendix A gives the Fourier series analysis of the transformer current, under ideal conditions. From this analysis, the dominant harmonic components at the design point, were computed as,

Primary current components:

$$I_1 = 430.3 \text{ Apk}$$

$$I_3 = 109.2 \text{ Apk}$$

$$I_5 = 32.7 \text{ Apk}$$

Secondary current components:

$$I_1 = 86.1 \text{ Apk}$$

$$I_3 = 21.8 \text{ Apk}$$

$$I_5 = 6.5 \text{ Apk}$$

Table 4.3.3 summarizes the copper losses, computed by the program, for each of the three arrangements - X, Y, Z. As a demonstration, Appendix B shows all the details required by the program, "TID", for arrangement Y. It is seen that the arrangement Y is the best, in terms of incurring least copper losses. The reduction in copper losses in going from arrangement X to Y can be explained as follows. A split up of the primary winding into two sections in Y, results in a peak field intensity half of that of X, in the window region. The ampere-turn waveform in the window region for the two winding arrangements is shown in Figure 4.3.3 to give an idea of the relative peak field intensities. Since, the proximity effect losses are proportional to the square of the leakage field, arrangement Y experiences lower proximity effect losses as compared to that of X. However, this does not explain the increased losses in arrangement Z, which is simply a different permutation of Y. To understand this a flux distribution of the three arrangements was generated using a magnetostatic finite element solver [ANSOFT package]. Figure 4.3.4 depicts the flux distribution for each arrangement in the absence of

TABLE 4.3.3

(Summary of Winding Losses in the three arrangements)

$(P_O = 50kW, V_1 = 200Vdc, V_O = 2000Vdc, f = 50kHz)$

	X	Y	Z
Primary(W)	179	144	301
Secondary(W)	97	32	297
	---	---	---
Total(W)	276	176	598
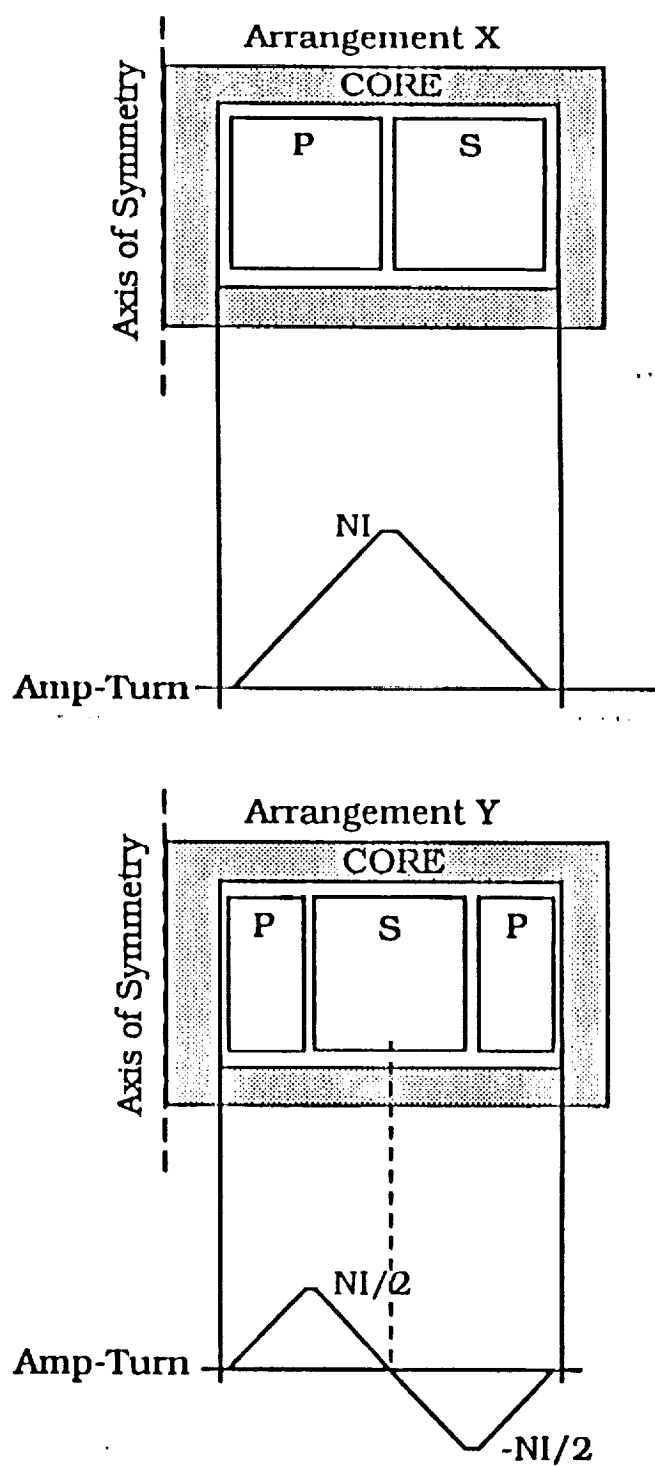
Figure 4.3.3 Idealized ampere-turn waveforms in the window region for winding arrangements X and Y

X

Axis of Symmetry
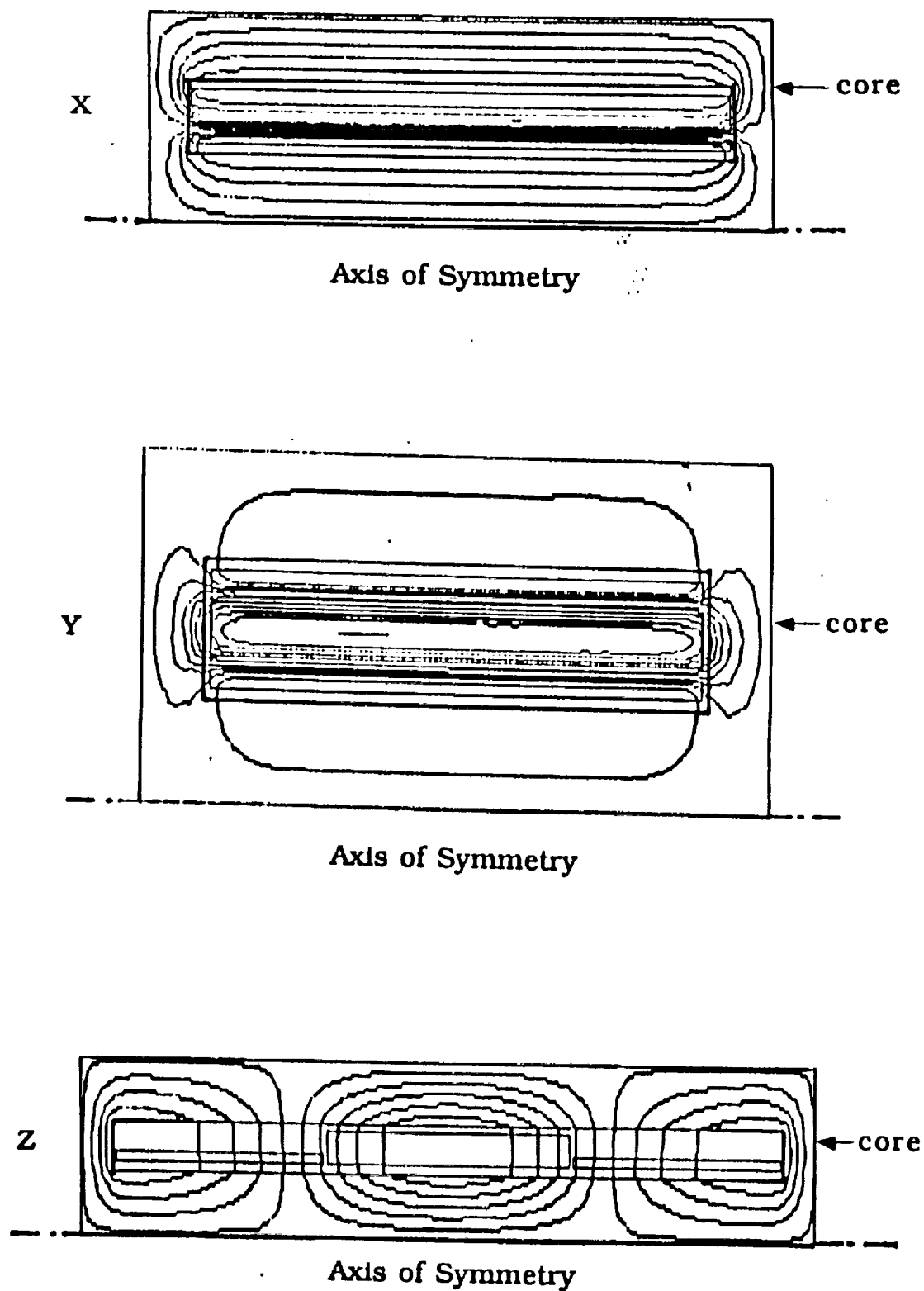
Y

Axis of Symmetry

Z

Axis of Symmetry

Figure 4.3.4   Leakage flux plots for the three conventional winding arrangements, obtained from magnetostatic finite element analysis

eddy currents. Recalling that the primary windings are foil-wound, in arrangement Z it is seen that the flux lines enter the primary foil-plane perpendicularly. Eddy currents are readily induced in the foil-plane, since a large surface area is available for conduction. These eddy currents, as a result of the pronounced proximity effect, give rise to the very large copper losses observed in Table 4.3.3.

In short, to minimize copper losses, windings must be sectionalized and interleaved to reduce field intensities in the window region. Moreover, these sections must also be arranged such that the flux lines are directed parallel to foil planes.

As seen from the flux plots for the conventional windings, a considerable amount of leakage flux gets coupled into the core. In designs where the leakage flux is small, it may not be very important. However, for converters where the leakage inductance is the main power transfer element, this could contribute substantially to localized saturation of the core, resulting in local hot spots and additional core losses. A preferred technique is the use of coaxially wound transformers, a well-known technology in the area of radio frequency magnetic component design [10, 11].

4.4 Coaxial Winding Arrangements

Figure 4.4.1a shows a coaxially wound transformer using conductors of circular cross-section, the simplest possible geometry for such transformers. The primary consists of a single turn made from a U-shaped tube of circular cross-section. The thickness of the tube must be maintained within a skin-depth, which as calculated before is 12 mils at 50 kHz. However, from the standpoint of mechanical rigidity the thickness of the tube needs to be atleast 2 to 3 times this value. The inner secondary winding is of litz wire. The preferred core geometry is toroidal. Multiple toroidal cores can be slipped on the primary winding, depending upon the core area desired.

Core
(Toroid)

Primary
(U-tube)

r_{p1}

r_s

Secondary
(Litz, N_S turns)

Exposed Portion
of secondary wdg.
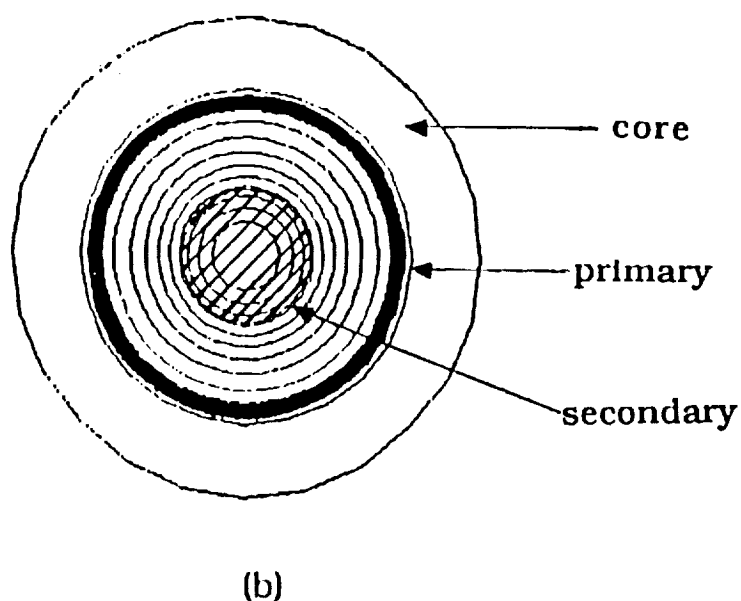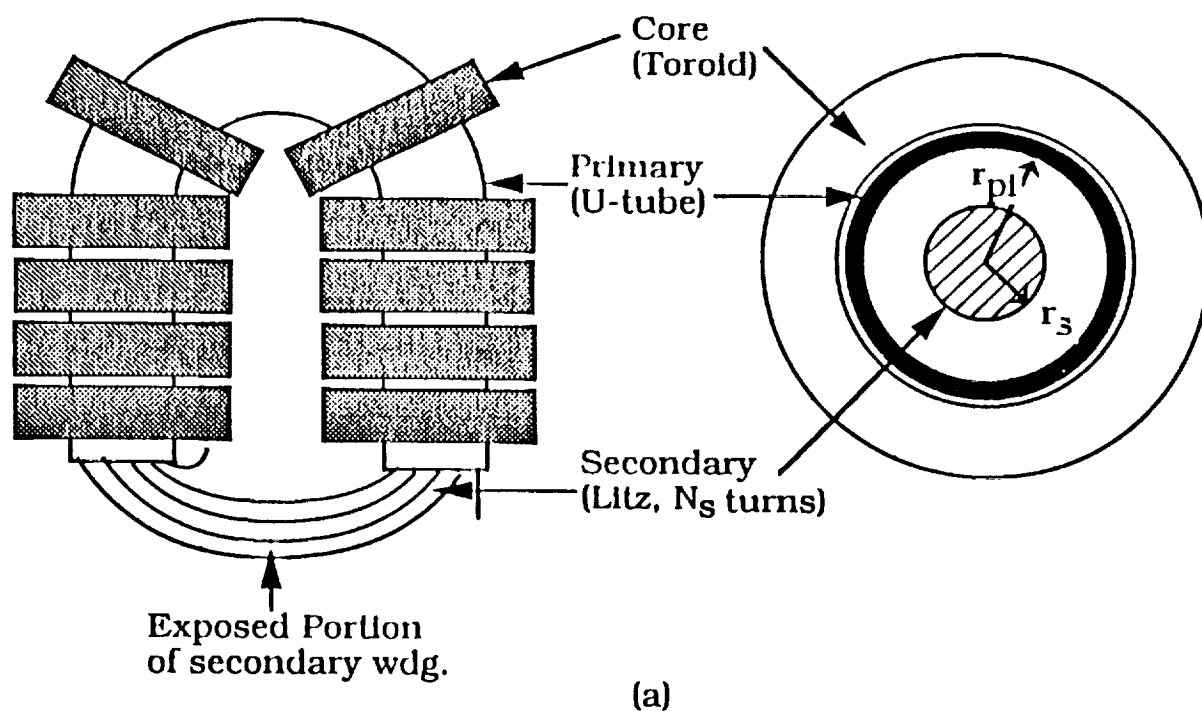
(a)

core

primary

secondary

(b)

Figure 4.4.1 (a) Coaxially wound transformer, with primary tube of circular cross-section. (b) Leakage flux distribution, from magnetostatic finite element analysis, showing all the leakage flux confined within the primary tube

A point worth mentioning here is with regard to the choice of core material. As far as conventionally wound transformers are concerned, it is seen that the optimum choice of core geometry is the shell-type built from E-E cores, for high power applications. This left us with Ferrite as the material of choice, given the unavailability of such shapes in the Permalloy80 tape-wound material for single-phase applications. On the other hand, for coaxial transformers with circular cross-section, a toroid is the optimum core geometry. Also, from a viewpoint of physical implementation, at higher power levels, the number of turns on the outer tubular winding gets limited to one. This would drastically lower the magnetizing inductance if Ferrite is used as the core material, for a given core cross-section. The much higher permeability of Permalloy80 tape-wound cores and their availability in toroidal shapes, does suggest the suitability of this material for coaxial transformers.

A flux plot for the above arrangement, under loaded conditions, is shown in Figure 4.4.1b. This was obtained using the magnetostatic finite element analysis software [ANSOFT]. As expected, the leakage flux is uniformly confined to the region inside the outer tube only. This is the flux due to the inner secondary winding. As mentioned earlier, this is certainly very desirable since the core is free from the effects of any localized saturation.

The leakage flux consists of the internal flux of the secondary winding and the flux within the interwinding space, which is linked by the secondary winding only. Hence, the leakage inductance per unit length can easily be derived as,

$$L_{cir} = \frac{N_s^2 \, \mu_0}{4\pi} \left[1 + 2 \ln(\frac{r_{pi}}{r_s}) \right] \text{ H/m} \qquad ...(4.4.1)$$

where, r_{pi} is the inner radius of the primary tube (outer conductor), and r_s is the radius of the secondary litz wire, and N_s is the number of secondary turns. It is seen from Equation (4.4.1) that for a given N_s as

the interwinding space is reduced by decreasing r_{pi}, the leakage inductance decreases. This is the most interesting feature of the coaxial winding, in that the leakage inductance is so easily controllable. In the above derivation, it is assumed that the inner winding is completely enclosed by the outer tubular winding. However, as shown in Figure 4.4.1a, this is not true. The portion of the inner winding that is not enclosed, simply contributes to the leakage inductance. If a high leakage inductance is desired, and the interwinding space is at a premium, then the length of the exposed inner winding can be judiciously controlled to achieve the objective.

The transformer is also very robust mechanically. The electromechanical forces on the windings, which could potentially be large enough to damage the transformer core at the high current levels expected, are lower than for conventional designs, as the leakage flux can be controlled and confined within the outer conductor.

Another coaxial winding geometry that is under investigation uses a primary conductor of rectangular cross-section. This facilitates the use of E-E cores, if Ferrites is the core material of choice. Figure 4.4.2a shows the top view of such a coaxial winding. Figure 4.4.2b shows its leakage flux distribution obtained from the magnetostatic finite element analysis, which assumes uniform current distribution. Under such conditions considerable amount of leakage flux would permeate the core, in particular at the corners of the tube, as seen from the flux plot. This is so, because of the asymmetry in the winding in the radial direction. However, in reality, the leakage fluxes entering or leaving the tube induce eddy currents, which by Lenz's law would tend to oppose this leakage field. The resultant effect, is a redistribution of the current in the outer tube, as shown in Figure 4.4.2c. Intuition says that the majority of the resultant leakage field would still stay confined within the outer tube. This proposition remains to be verified, from an eddy current finite element analysis.
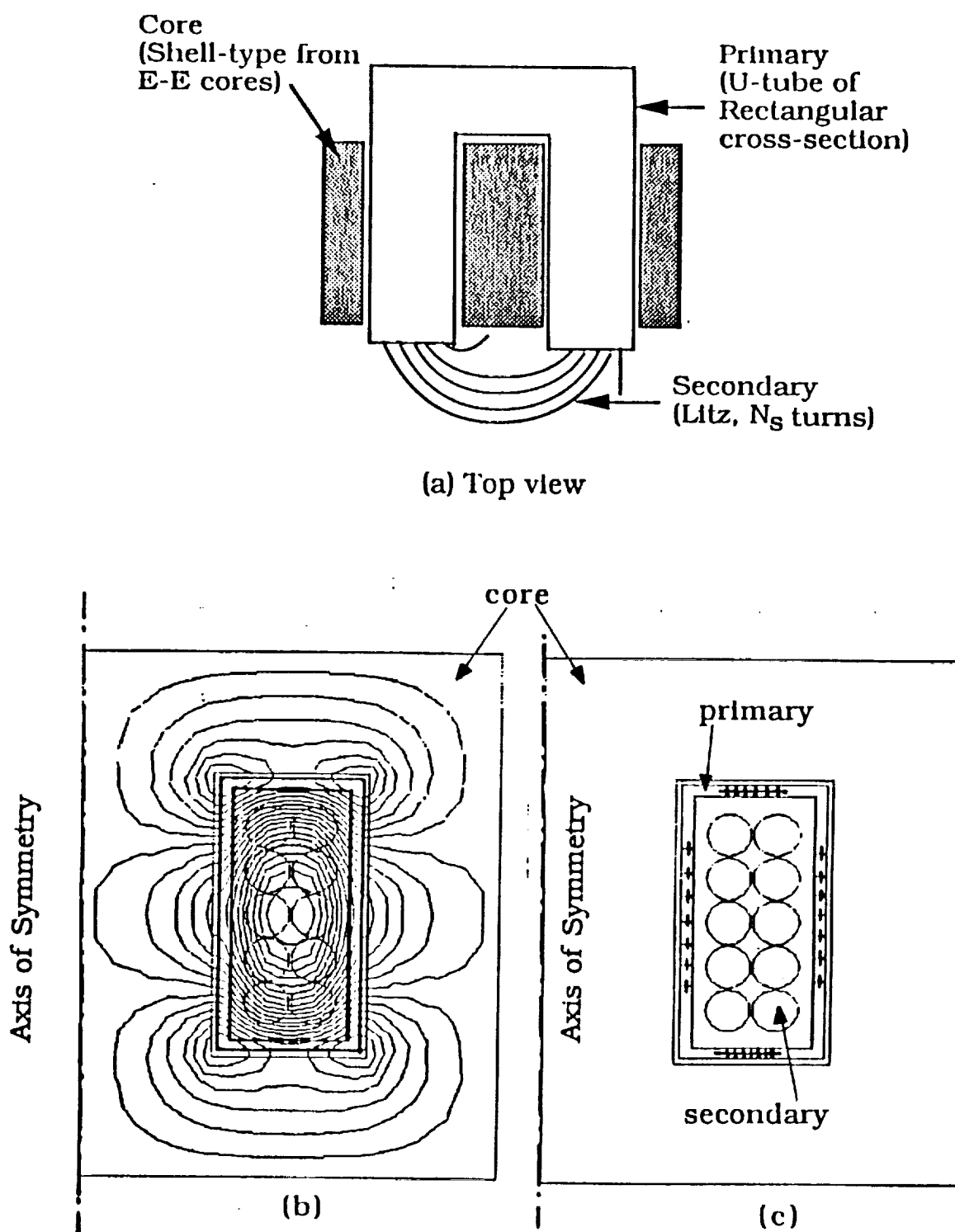
(a) Top view

Figure 4.4.2   (a) Coaxially wound transformer, with primary tube of rectangular cross-section. (b) Leakage flux distribution. (c) Redistribution of current in the primary conductor due to eddy currents

4.5 Experimental Results on Two Coaxially Wound Transformers

4.5.1 Rectangular Coaxial Geometry

Figure 4.5.1 shows a vertical cross-section of the transformer fabricated in the laboratory. Fundamentally, the transformer construction is that of the standard shell-type. Two secondary windings are wound inside a copper tube of rectangular cross-section. The details of the transformer are listed below.

Core

Material:	Ferrite PC40 (manufacturer : TDK, Part No. EI70)
Shape:	E-E, 3 pairs
Core Area:	2.125×10^{-6} m^2
Core Volume:	502.7×10^{-6} m^3
Bmax:	0.15 T
Weight:	2.413 kg

Windings

Primary:	1 winding
Conductor Type:	Copper Rectangular tube
No. of turns:	3
Wall thickness:	1000 µm = 3δ, δ=305 µm is skin depth at 50 kHz
Current density:	4.46×10^6 A/m^2

Secondary:	2 windings
Conductor Type:	Litz wire, AWG 10, 660 strands, 5x3/44/38
No. of turns:	15 each
Current density:	5.83×10^6 A/m^2

Insulation:

Epoxy:	Inside walls of primary tube
Kapton:	Between secondary windings, 5 mils (1mil=25.4 µm)

Window Fill Factor:	40% (extra insulation required for high voltages)
Total Weight:	3.834 kg

SECONDARY
WINDING # 2
(LITZ, 15T)

SECONDARY
WINDING # 1
(LITZ, 15T)

PRIMARY
(COPPER TUBE, 3T)

COPPER STRAP

CORE
(FERRITE PC40, E-E)

INSULATION

VERTICAL CROSS-SECTION
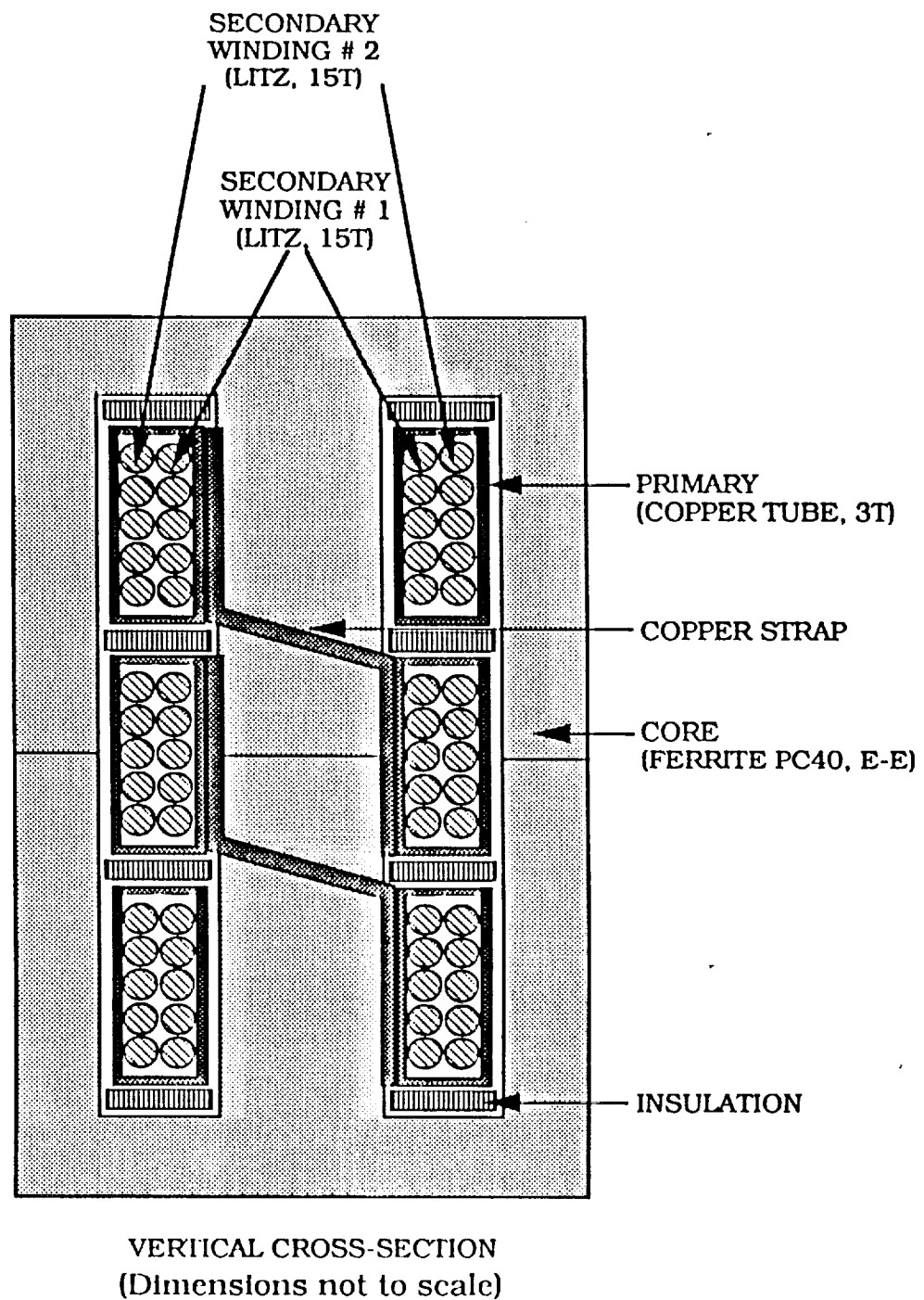(Dimensions not to scale)

Figure 4.5.1   Coaxially wound transformer, with rectangular tube for
the primary winding, fabricated in the laboratory

The open circuit and short circuit tests at 50 kHz were performed on the transformer. Test results are presented below. Figure 4.5.2 is a photograph of the transformer built in the laboratory. Figure 4.5.3 shows oscillograms of the transformer secondary voltage and primary current under short circuit test conditions.

Test Data for Rectangular Coaxial Transformer

Magnetizing Inductance (primary referred) = 250 μH

Leakage Inductance (primary referred) = 150 nH

DC Resistance of Primary Winding = 0.289 mΩ

DC Resistance of Secondary Winding # 1 = 22.17 mΩ

DC Resistance of Secondary Winding # 2 = 23.57 mΩ

Shunt Capacitance (primary side) = 1 nF

Open Circuit Core Losses = 70W at 200Vrms (primary), 0.15T, 50 kHz

Short Circuit Copper Losses = 180 W at 230 Arms on primary

Total Losses = 250W at projected kVA of 200Vrms x 230Arms=46 kVA

Projected Efficiency (at 46 kVA) = 99.4 %

Projected Power Density (at 46 kVA) = 0.083 kg/kW
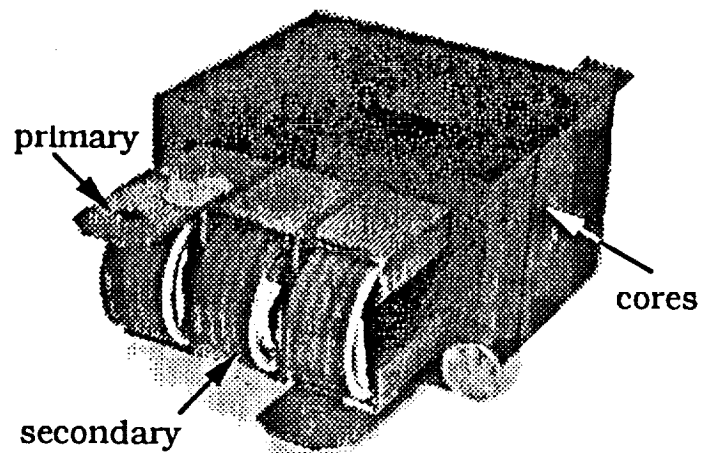
Figure 4.5.2   Photograph of fabricated 50 kVA, 50 kHz, coaxially wound transformer, with **rectangular** tube for the primary winding

Top Trace: Secondary voltage, 50 V/div
Bottom Trace: Primary Current, 100 A/div

f 50.00 kHz   T/div 5 µs
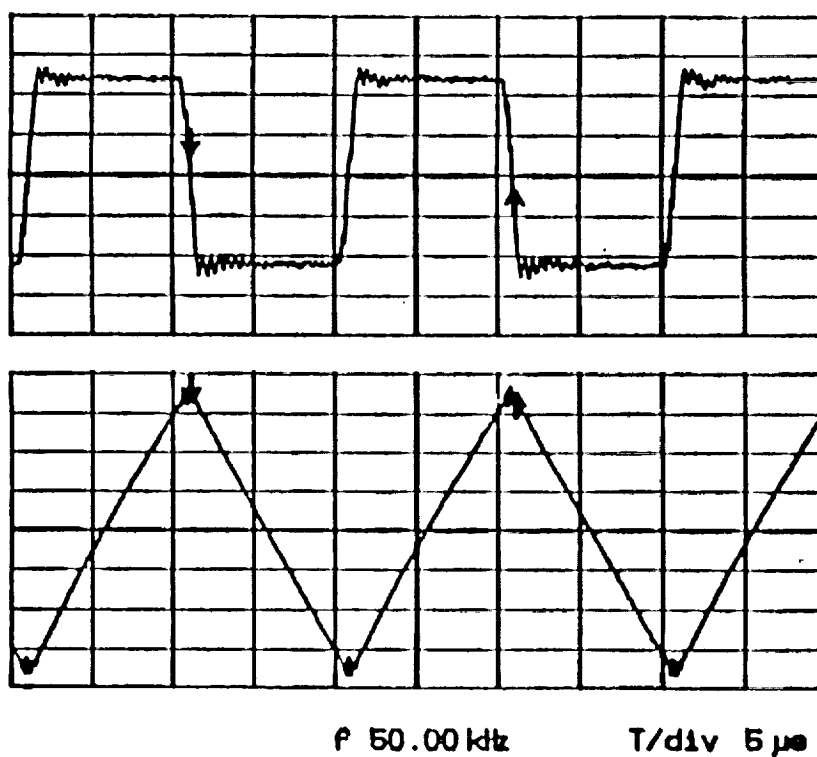
Figure 4.5.3   Oscillograms under short circuit test conditions, for the
                50 kVA, 50 kHz coaxially wound transformer with
                rectangular tube for the primary winding

4.5.2 Circular Coaxial Geometry

Figure 4.5.4 is a photograph of a coaxially wound transformer with circular primary tube. As mentioned earlier, although, Permalloy80 would be an ideal candidate for such a geometry because of its higher permeability, lower specific core losses at 50 kHz and availability in toroidal shapes, the core material used in the prototype is Ferrite primarily for cost reasons. The details of the transformer are given below.

Core

Material:	Ferrite PC30 (manufacturer : TDK, T68 x 16.5 x 44)
Shape:	Toroid, 26 peices
Core Area:	$5.148 \times 10^{-3} \ m^2$
Core Volume:	$906 \times 10^{-6} \ m^3$
Bmax:	0.15 T
Weight:	4.368 kg

Primary Winding: 1 winding

Conductor Type:	Copper Circular tube
No. of turns:	1
Wall thickness:	1000 μm = 3δ, δ=305 μm is skin depth at 50 kHz
Current density:	$1.90 \times 10^6 \ A/m^2$

Secondary Windings: 2 windings

Conductor Type:	Litz wire, AWG 10, 660 strands, 5x3/44/38
No. of turns:	5 each
Current density:	$5.83 \times 10^6 \ A/m^2$

Insulation:

Teflon:	Inside walls of primary tube
Kapton:	Between secondary windings, 5 mils (1mil=25.4 μm)

|	
Window Fill Factor:	15% (intentionally low for higher leakage inductance)
Total Weight:	6.25 kg

primary ·   cores   secondary
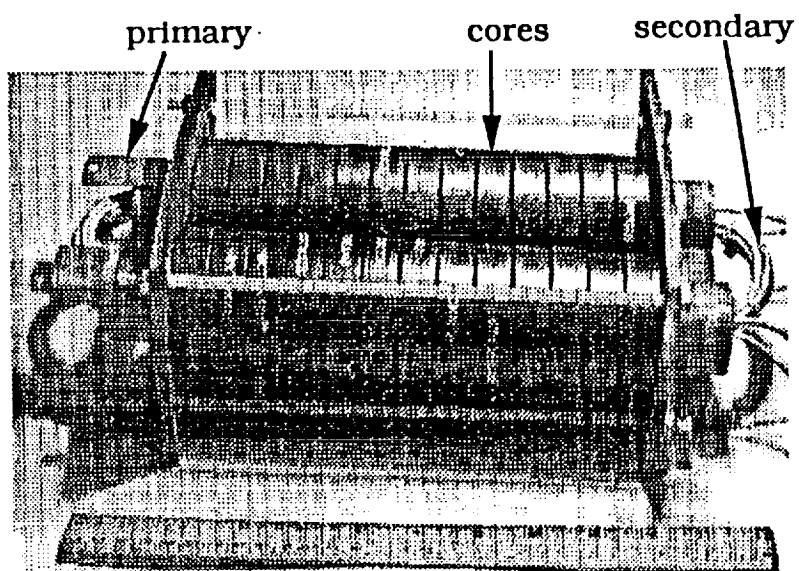
Figure 4.5.4   Photograph of fabricated 50 kVA, 50 kHz, coaxially wound transformer, with **circular** tube for the primary winding

Test Data for Circular Coaxial Transformer
(Not fully tested due to limitations in test set-up)

Magnetizing Inductance (primary referred) = 120 µH

Leakage Inductance (primary referred)

     Measured = 250 nH

     Calculated = 182 nH (from Eqn. 4.4.1)

Open Circuit Core Losses = 32.6W at 0.1 T, 50 kHz

Short Circuit Copper Losses = 42.2 W at 120 Arms on primary

To conclude, coaxially wound transformers are seen to be a viable alternative for the realization of high-power high-frequency transformers. Such transformers can realize multiple benefits of a low distributed and controllable leakage inductance, robust construction, low electromechanical forces and low core and copper losses. The prototype coaxially wound transformers fabricated in the laboratory demonstrate the feasibility of realizing very low leakage inductances, in the order of a few hundreds of nanohenries. Foreseeing the tremendous potential of coaxial transformers for high power density converters, it is hoped that a design methodology for such transformers would indeed be a valuable tool and will be pursued as part of the future work.

CHAPTER 5

CONCLUSIONS AND FUTURE WORK

5.1 Summary

The goal of this project is the development of a high power density, high power dc/dc converter for aerospace applications. The rated specifications are an output power of 50 kW, at an input voltage of 200 Vdc, output voltage of 2000 Vdc, with a power density of 0.2 - 0.3 kg/kW. The switching frequency will be in the order of 50 - 100 kHz.

Three new dc/dc converter topologies are proposed, namely

a) Phase-Shifted Single Active Bridge DC/DC Converter(Topology A)
b) Single Phase Dual Active Bridges DC/DC Converter(Topology B)
c) Three Phase Dual Active Bridges DC/DC Converter(Topology C)

The salient features of these topologies are :

1) All are minimal in structure, i.e., each consists of an input and output bridge, input and output filter and a transformer, all components essential for a high power dc/dc conversion process.

2) All devices of both the bridges can operate under near zero-voltage conditions, making possible a reduction of device switching losses and hence, an increase in switching frequency.

3) All circuits operate at a constant frequency, thus simplifying the task of the magnetic and filter elements.

4) Since, the leakage inductance of the transformer is used as the main current transfer element, problems associated with the diode reverse recovery are eliminated. Also, this mode of operation allows easy paralleling of multiple modules for extending the power capacity of the system.

5) All circuits are least sensitive to parasitic impedances, infact the parasitics are efficiently utilized.

6) The soft switching transitions, result in low electromagnetic interference.

In addition, the dual active bridge topologies can realize,

1) Two-Quadrant operation
2) Buck-boost characteristics
3) Low device and component stresses.

A detailed analysis of each topology has been carried out. The various steady state operating characteristics including, output voltage, power transfer, transformer utilization and filter capacitor kVA ratings as a function of the control and load parameters are presented for soft-switching conditions.

Based on the analysis, the various device and component ratings for each topology operating at an optimum point, and under the given specifications, are tabulated in Table 2.2.1. Topology A offers the possibilty of realizing high output voltages given the fact that the output is a diode bridge. However, the input filter capacitor ratings and device stresses are much higher than those for Topologies B and C. Moreover, the transformer utilization is the poorest. On the other hand, Topologies B and C exhibit device VA stresses which are only 20% higher than that of an ideal conventional hard switched pwm converter. Topology B gives a 40% improvement in the transformer utilization over that of Topology A. Topology C shows a similar improvement in the transformer utilization, at the expense of a more

physically complex symmetrical three phase transformer. As expected, the filter capacitor ratings for Topology C are the lowest.

Based on the following considerations, Topology B is selected as the final converter topology :

1) Allows better control range, under soft-switching conditions, as compared to Topology A, especially at a dc conversion ratio of unity

2) Relatively, simpler transformer design as compared to Topology C

3) Given the state-of-the-art in the high power density multi-layer ceramic capacitors, it is seen that very little or no weight penalty will be incurred, although the filter kVA requirements are higher than that those for Topology C

4) Requires fewer active devices compared to Topology C, and hence fewer drive circuits

5) Exhibits lowest device conduction and switching losses

6) Since the control methodology for Topology A can also be incorporated in Topology B, a much wider range of control can be achieved.

A fundamental component for the dual active bridge topologies is also presented, and it shows good correlation to the actual model. This model allows a better appreciation of soft switching constraints through phasor diagrams.

The region of soft switching available on the output voltage vs output current plane depends on the system parameters. In particular, it has been shown for Topology B that for low magnetizing inductance of the transformer, the region of soft switching widens at low loads.

However, the penalty is additional VA/watt. Also, for increasing values of the device snubber capacitance, although the device switching losses decrease, the soft switching region on the VA plane gets restricted.

Another area of emphasis, in this proposal, has been on the design considerations for high-power, high-frequency transformers. Various high frequency core materials have been experimentally characterized, based on specific core losses at different frequencies. Ferrite (PC40) and Permalloy80 (0.5mil) core materials show a lot of promise in the frequency range of interest. Investigation of conventional winding arrangements, has shown that copper losses in the transformer are extremely sensitive to the leakage flux distribution in the window region. Coaxially wound transformers are also seen to be a viable alternative for the realization of high-power high-frequency transformers. Such transformers can realize multiple benefits of a low distributed and controllable leakage inductance, robust construction, low electromechanical forces and low core and copper losses. Two such transformers, one with a rectangular tube and the other with a circular tube for the primary winding have been fabricated and tested in the laboratory. The leakage inductance measured for the the two transformers are in the order of a few hundreds of nanohenries only!!

5.2 Experimental Results from Proof-of-Concept Unit

An experimental proof-of-concept unit based on the proposed single phase dual active bridges dc/dc converter was fabricated in the laboratory, early during Phase 2 of the project, to verify some of its theoretically predicted steady state operating characteristics. Figure 5.2.1 shows the schematic of the unit rated for 1 kW for a switching frequency of 20 kHz. The switching devices used were BJTs(darlington). The single phase core-type transformer was constructed from Permalloy80(2 mil) tape-wound core. The transformer was wound for a turns ratio of 1 : 2, using foil for the primary winding and litz wire for the secondary.

The input and output bridges were phase-shifted from each other in an open-loop manner. The objective of this excercise was to study the power transfer versus control characteristics, and efficiency performance. Figure 5.2.2 shows the primary and secondary voltage waveforms and the primary current waveforms for $d = 1$. The waveforms demonstrate the soft-switching capabilities for all the devices on both the bridges. Figure 5.2.3a shows the variation in output power with the control variable, ϕ. The parameter d was set to unity. Due to limitations in the controller, the phase-shift could not be varied over a wider range. The theoretical curve is also superimposed on the same figure. The trend in the experimental curve is seen to closely match that of the theoretical. Output power increases as ϕ increases. Note, the theoretical curve assumes 100% efficiency. This would explain the discrepancy in the theoretical and experimental output power for each phase-shift.

Figure 5.2.3b shows the variation in the transformer kVA with output power for the same conversion ratio. Again, the experimental results are seen to be in close agreement with theory. Figure 5.2.3c shows the efficiency versus phase-shift plot. A maximum efficiency of 73% was obtained.

It is seen that the proof-of-concept unit does demonstrate the feasibility of the proposed dc/dc converter. The theoretically obtained power transfer characteristics are reasonably well corroborated by experiment, which was the main objective.
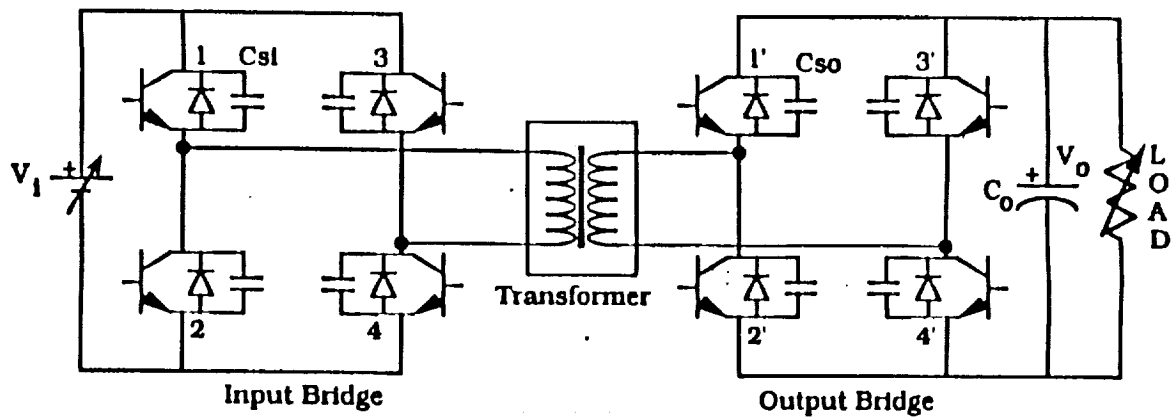
Device: 1200V, 150A, Dual Darlington BJT

Transformer: 1 Phase, Core-type, 1kVA, 20kHz, 200V, 1:2
Core: Permalloy80, 2mil

Csi: Input Device Snubber Capacitor, 0.2μF, Silver-Mica

Cso: Output Device Snubber Capacitor, 0.1μF, Silver-Mica

Figure 5.2.1   Experimental proof-of-concept unit rated for 1 kW at a switching frequency of 20 kHz. Note the semiconductor devices and transformer construction and core material used
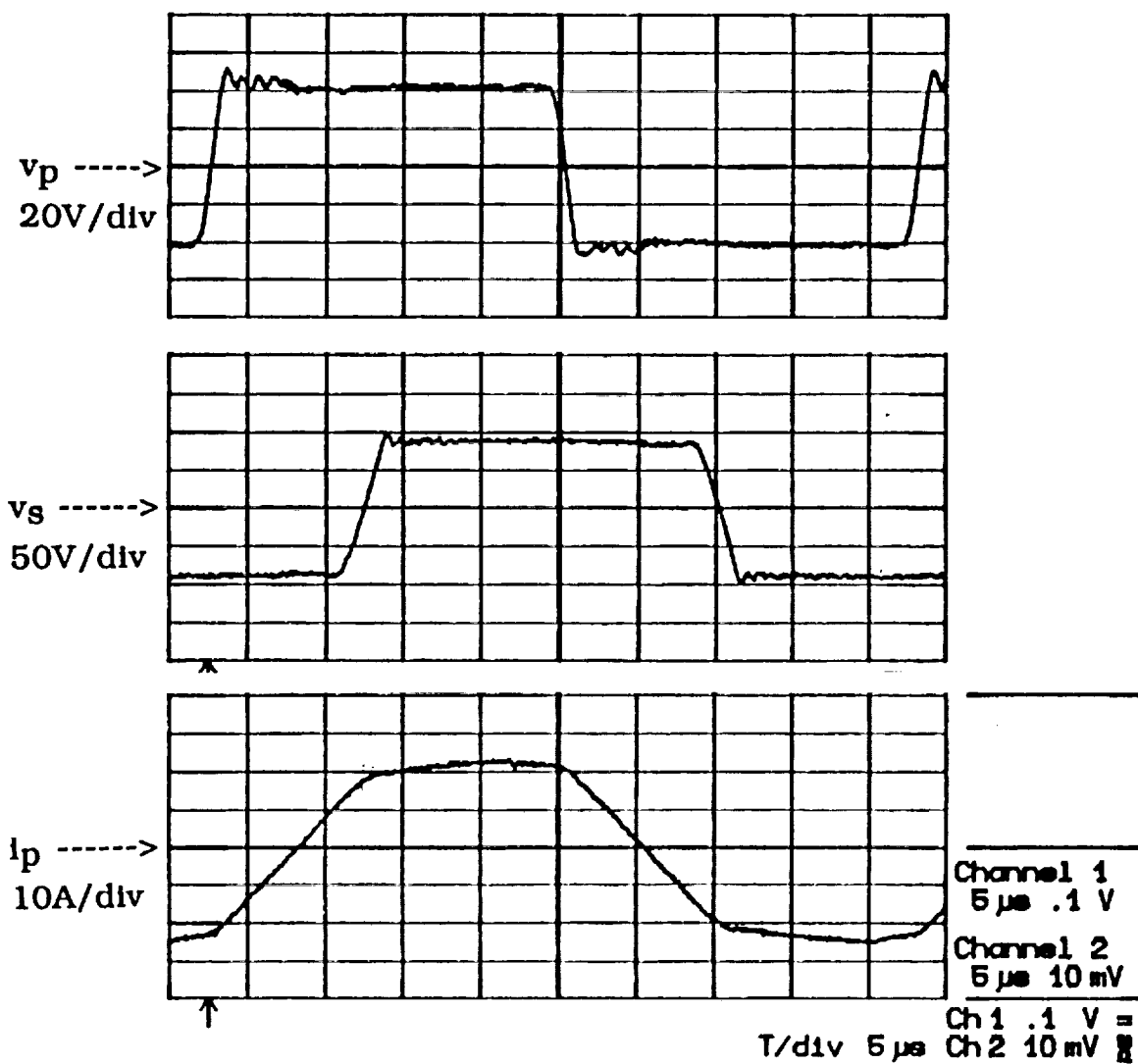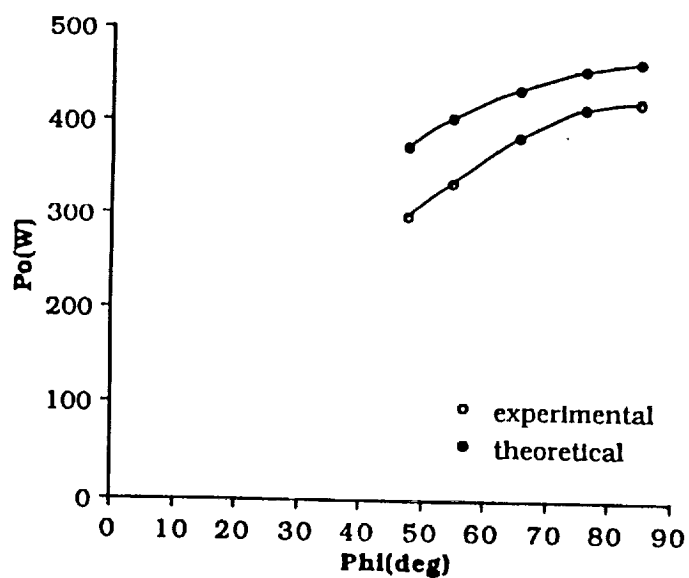
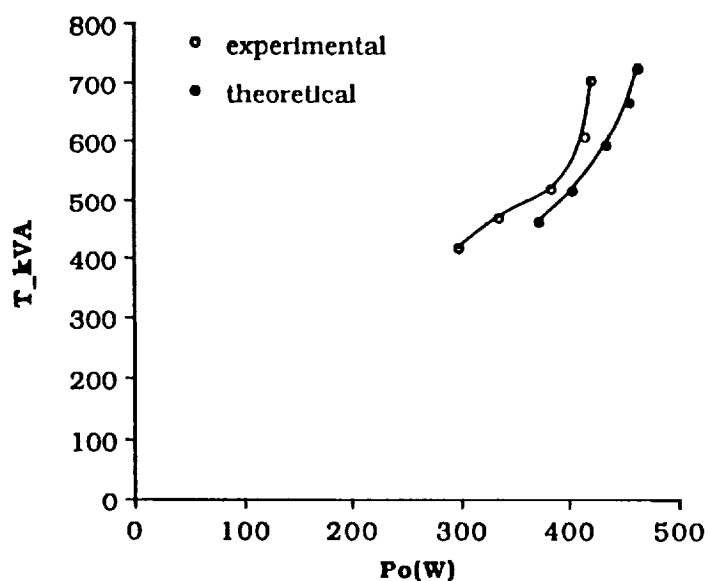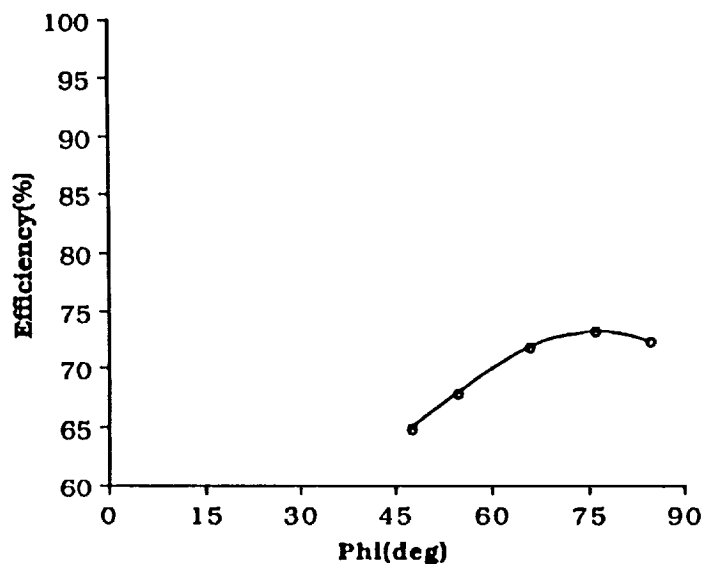**Figure 5.2.2** Experimental waveforms of the transformer voltages and current, demonstrating soft switching capability of proposed converter

Figure 5.2.3 Experimental and Theoretical operating characteristics of the proposed converter (Topology B), for d=1. (a) Output power vs phase-shift. (b) Transformer kVA vs output power. (c) Efficiency vs phase-shift

5.3   Future Work

The tasks involved in the future phase of this project include the following:

1)Fabrication of a 50kW, IGBT unit based on the proposed Topology B, for an input dc voltage of 200V and output dc voltage of 2000V. To meet the high output voltage requirement, two half-bridges will be connected in series, as shown in Figure 2.5.1. The initial choice of switching frequency is 50kHz, with a hope of reaching 100kHz.

As stated earlier, the leakage inductance of the transformer is the main energy transfer element, and hence, needs to be tightly controlled. To realize this objective a coaxially wound transformer, schematic of which is shown in Figure 4.4.3, has been fabricated and will be tested.

A significant portion of the overall power density is associated with the filter capacitors. The size of these capacitors is governed, mainly by the rms currents flowing through them. Traditionally used commutation-grade capacitors tend to be bulky and lossy. The recently introduced multi-layer ceramic(MLC) capacitors offer much higher power densities and will be investigated for our application.

Overall circuit layout issues for good thermal management, low parasitic impedances and low volume will also be addressed.

2)Digital simulation of a "current-programmed" controller for output voltage regulation is currently underway. The converter will be operated under current mode to ensure parallel operation of multiple units.

3)Derivation of a small signal model to understand the frequency response characteristics of the proposed converter, especially under a current mode control.

4)Coaxially wound transformers seem to possess many desirable features including low and distributed leakage inductance, low core

and copper losses and high power density. A design methodology for such transformers, specifically tuned to the above requirements, will be pursued.

5)Topology C will be analyzed in detail and a 3 phase coaxial transformer design will be developed.

REFERENCES & BIBLIOGRAPHY

[1] M. H. Kheraluwala, D. M. Divan, "High Power Density DC/DC Converter - Selection of Converter Topology", NASA Interim Report No. 1, Grant No. NAG3-804, July 1987 - June 1988.

[2] M. H. Kheraluwala, D. M. Divan and E. Bauman, "Design Considerations for High Power Density DC/DC Converters", High Frequency Power Conversion Proceedings, 1990.

[3] A. Mertens and D. M. Divan, "A High Frequency Resonant DC Link Inverter Using IGBTs", to be presented at IPEC-90, Tokyo.

[4] Toshiba Power Semiconductor Databook, 1989.

[5] MCT Workshop Conference Proceedings, Schenectady, New York, November 1988.

[6] J. Lammeraner and M. Stafl, "Eddy Currents", Iliffe Books-London, 1966.

[7] R. L. Stoll, "The Analysis of Eddy Currents", Clarenden Press - Oxford, 1974.

[8] J. A. Ferriera, "Electromagnetic Modelling of Power Electronic Converters Under Conditions of Appreciable Skin and Proximity Effects", Ph.D. Thesis, Rand Afrikaans University, Johannesburg, South Africa, Nov. 1987.

[9] K. J. Binns and P. J. Lawrenson, "Analysis and Computation of Electric and Magnetic Field Problems", Pergamon Press, published in 1963.

[10] G. Guanella, "Novel Matching Systems for High Frequencies", Brown-Boveri Review, vol. 31, Sep. 1944, pp. 327-329.

77

[11] E. G. Fubini, P. J. Sutro, "A Wide-Band Transformer from an Unbalanced to a Balanced Line", Proc. IRE, vol. 35, Oct. 1947, pp. 1153-1155.

[12] M. H. Kheraluwala, D. W. Novotny and D. M. Divan, "Design Considerations for High Power High Frequency Transformers", to be presented at the IEEE-Power Electronic Specialists Conference at San Antonio, June 1990.

Fourier Series Analysis of the Transformer Primary Current for Topology B

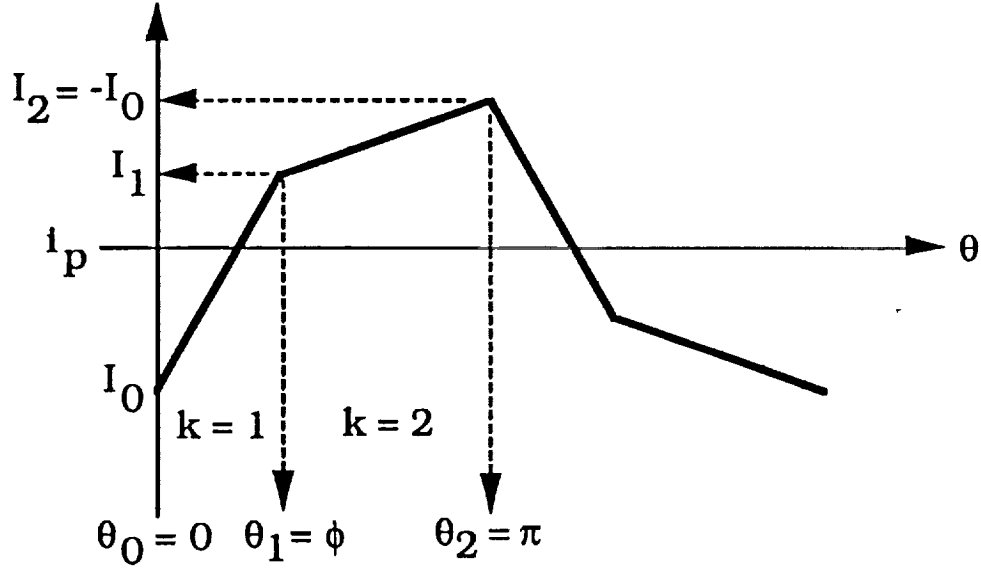Figure A.1   Typical transformer primary current

Figure A.1 shows a typical waveform for the primary current, $i_p(\theta)$, through the transformer, which is modelled simply by its leakage inductance, for Topology B. In each mode, the segment of the current is linear, and hence can be mathematically expressed, in general, as

$$i_k(\theta) = m_k (\theta - \theta_{k-1}) + c_k \qquad \qquad ...(A.1)$$

where, k is the mode no.,

m_k is the slope of the current segment in the kth mode, given as,

$$m_k = \frac{I_k - I_{k-1}}{\theta_k - \theta_{k-1}} \qquad \qquad ...(A.2a)$$

$$c_k = I_{k-1} \qquad \qquad ...(A.2b)$$

I_{k-1}, I_k, θ_{k-1} and θ_k are the initial and final values of the current and θ for the kth mode.

The Fourier Series coefficients for the above current are given as,

$a_0 = 0$,   since the average value is zero.

$$a_n = \frac{2}{\pi} \left[\int_0^\phi \{m_1(\theta) + c_1\} \cos(n\theta)\, d\theta \right.$$

$$\left. + \int_\phi^\pi \{m_2(\theta - \phi) + c_2\} \cos(n\theta)\, d\theta \right] \qquad \text{for } n = 1, 2...$$

$$...(A.3a)$$

$$b_n = \frac{2}{\pi} \left[\int_0^\phi \{m_1(\theta) + c_1\} \sin(n\theta)\, d\theta \right.$$

$$\left. + \int_\phi^\pi \{m_2(\theta - \phi) + c_2\} \sin(n\theta)\, d\theta \right] \qquad \text{for } n = 1, 2...$$

$$...(A.3b)$$

where, m_k and c_k are as defined in Equations (A.2a) and (A.2b).

Substituting for the m_k's and c_k's and carrying out the necessary algebra we get,

$$a_n = 0 \qquad \text{for n even}$$

$$a_n = \left[\frac{2}{\pi n^2}\right]\left[\frac{(I_1 - I_0)\cos(n\phi - 1)}{\phi} + \frac{(I_1 + I_0)\cos(n\phi + 1)}{(\pi - \phi)}\right]$$

$$\text{for n odd} \qquad ...(A.4)$$

Now, from Equations (3.3.5) and (3.3.6) (Chapter 3 of Reference 1)

$$I_0 = -\frac{V_1}{2\omega L}\left[2d\phi + \pi(1 - d)\right] \qquad ...(A.5a)$$

and,

$$I_1 = \frac{V_1}{2\omega L}\left[2\phi - \pi(1 - d)\right] \qquad ...(A.5b)$$

Substituting the values of I_0 and I_1 from Equations (A.5a) and (A.5b) into Equation (A.4) and simplifying, we get,

$$a_n = \frac{4V_1}{\pi\omega L n^2}\left[d\cos(n\phi) - 1\right] \qquad ...(A.6)$$

Similarly,

$$b_n = 0 \qquad \text{for n even}$$

and,

$$b_n = \frac{4V_1}{\pi\omega L n^2}\left[d\,\sin(n\phi)\right] \qquad \text{for n odd} \qquad ...(A.7)$$

The amplitude of the nth odd harmonic can now be expressed as,

$$c_n = \sqrt{a_n^2 + b_n^2}$$

$$= \frac{4V_1}{\pi\omega L n^2}\sqrt{d^2 - 2d\cos(n\phi) + 1} \qquad ...(A.8)$$

For d = 1, we get from Equation (A.8),

$$c_n = \frac{8V_1}{\pi\omega L n^2}\sin(\frac{n\phi}{2}) \qquad n = 1, 3, 5... \qquad ...(A.9)$$

Figure A.2 shows the variation of the first four significant harmonics with ϕ, over the range 0 to $\pi/2$, for d = 1.
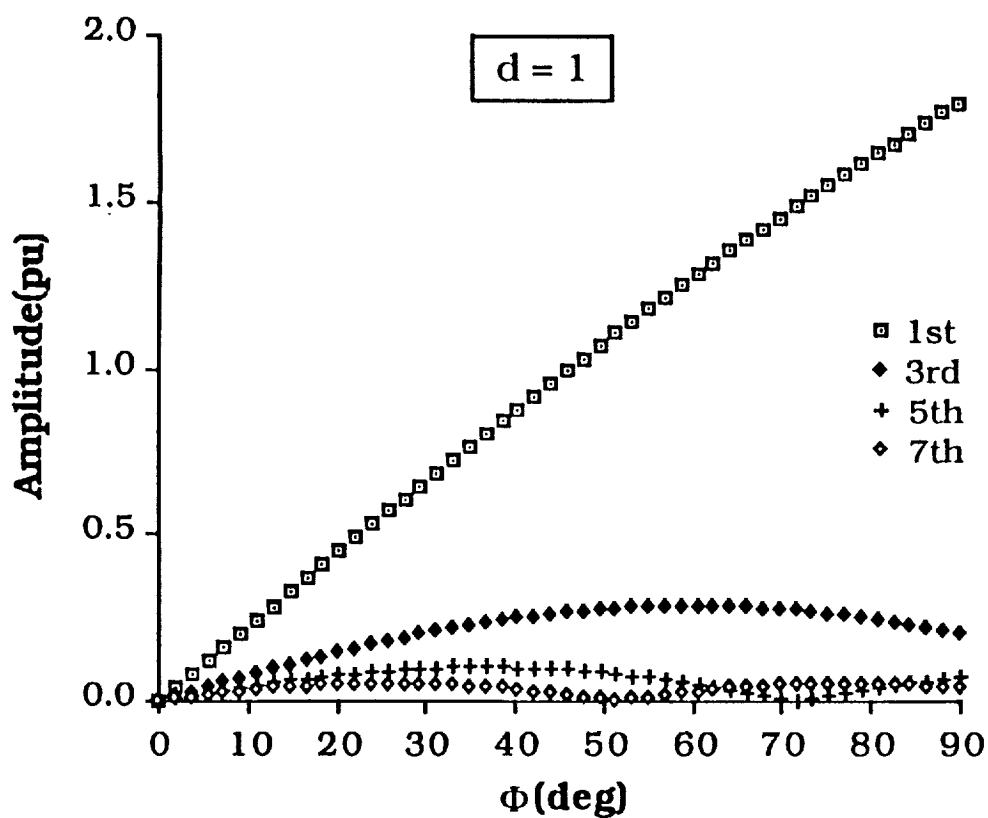
Figure A.2   Current harmonic amplitudes as a function of ϕ. The amplitudes are normalized to the current base, $I_b = V_1/\omega L$.

APPENDIX B
Demonstration of usage of "TID"

TRANSFORMER AND INDUCTOR WINDING DESIGN - VERSION 1A
COPYRIGHT - RAU, 1989
Author - Braham Ferreira

Output Control:
    Total Power Dissipation   <===
    Effective Resistance
    Power Dissipation Density Plot
    Magnetic Field Intensity Plot

SUB-MENU FOR GENERAL CONFIGURATION
Magnetic Core Parameters:
    Permeability (relative to air) of core = 2.5E+0003
    Diameter of Centre Leg of Core = 0.07497m
    Closed Window Ratio(percentage) = 52.00
    Open Window Ratio(percentage) = 48.00
    Airgaps (Number = 0,1 or 2) = 0

Window Dimensions:
    Height of Window = 0.01166m
    Width of Window = 0.15814m

Frequency Components:
    First Harmonic = 5.0E+0004
    Quantity of frequency components (maximum of 9) = 3

SUB-MENU FOR WINDING CONFIGURATION
Number of winding sections = 2

Winding Sections
1: Bottom coordinates=(0.0013,0.0013)   Top coordinates=(0.1569,0.0032)
    Turns=(1x3)   Type: COPPER,Monofilar,Strip(0.00051m,0.15560m)
    Current=(430.300,109.200,32.700)A
2: Bottom coordinates=(0.0345,0.0044)   Top coordinates=(0.1236,0.0104)
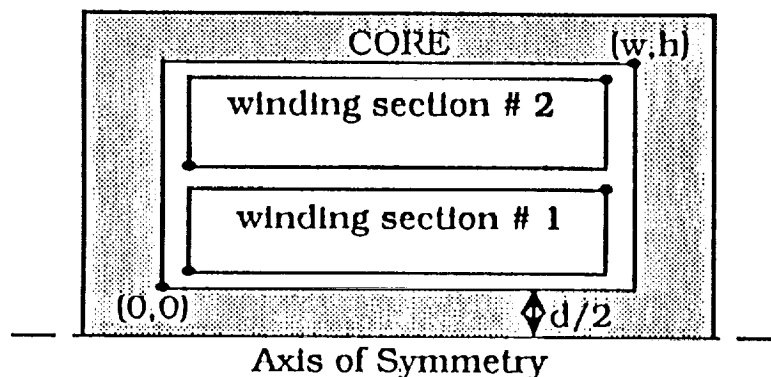   Turns=(15x1)   Type: COPPER,Monofilar,Litz(0.00582m,0.00013m,1050)
    Current=(-86.100,-21.800,-6.500)A

Figure B.1 Winding Arrangement X